Simulating the Next International Linear Collider Large Detector

Michael D. Duckwitz

December 5, 1999

Abstract

The next international linear collider has been proposed by physicists from Europe, Japan and the United States to study extensions to the current model of fundamental particles and forces. By performing simulations of the particle detector we are able to determine an effective detector geometry of minimum cost. These simulations study the resolution and calibration of one part of the detector—the calorimeter. There are two main proposed geometries, the Large and Small detectors. The feasibility of the Small detector will be assessed by considering the layer thicknesses, materials used and the effects of a magnetic field.

Contents

List of Figures

1 Introduction

The next quarter century in high energy physics (HEP) will be used to research extensions to the Standard Model. New theories in HEP are tested using particle colliders. Many high energy physicists will help in the research and development of the next linear particle collider during the next decade. Our topic of interest is the ideal geometry for the detector used with this collider. A computer simulation software package called GEANT is used for this process.

The Standard Model (SM) is the name given to the collection of knowledge we have of fundamental particles and the interactions among them. In spite of the great success of the SM, it predicts a divergent mass for the Higgs particle (as described below) and does not account for the force of gravity.

1.1 The Standard Model

According to the Standard Model, all matter is made of twelve particles and these particles interact via four fundamental forces. The twelve particles are subdivided into leptons and quarks as displayed Table 1. Quarks mainly differ from leptons in that they may interact strongly (i.e. exchange gluons). Table 2 shows the four forces and the associated propagators. In quantum theory, interactions take place by exchanging these force propagators. For example, two electrons electrically repel one another by exchanging photons.[1]

Particles have an intrinsic property called spin angular momentum (simply referred to as spin). The spin of a particle may be thought of classically as a spherical particle spinning on an axis like the Earth does. Spin is measured in units of angular momentum and is equal to $\sqrt{\hbar^2 s(s+1)}$ where $\hbar \equiv h/2\pi$, $h = 6.626 \cdot 10^{-34}$ joule-seconds (Planck's constant) and s is the spin quantum number. Often, the spin of a particle is simply said to be s. For instance, the electron is a particle of spin quantum number $s = \frac{1}{2}$ and is called a spin $\frac{1}{2}$ particle. Particles with integer spin (e.g. 0 or 1) are called bosons and particles with half-integer spin (e.g. $\frac{1}{2}$ or $\frac{3}{2}$) are called fermions.

As mentioned above, the standard model is not complete. The Higgs field is theorized to account for the masses of all the particles via the interaction with the Higgs particle. This Higgs *mechanism* (which is simply an additional interaction in nature) has not been verified and the Higgs particle has not

---

[1] Photons are quanta, or packets, of electromagnetic radiation.

Table 1: Quarks and leptons of the Standard Model

Leptons	Electron (e) Electron Neutrino (ν_e)	Muon (μ) Muon Neutrino (ν_μ)	Tau (τ) Tau Neutrino (ν_τ)
Quarks	Up (u) Down (d)	Charm (c) Strange (s)	Top (t) Bottom (b)

Table 2: Interactions of the Standard Model

Interaction	Strong	Electromagnetic	Weak	Gravitation
Propagator	Gluon	Photon	$W^{\pm}$, Z^0	Graviton

been discovered. However, one may calculate what the mass of the Higgs particle should be from its couplings with the particles of the SM. When the mass of the Higgs particle is calculated, it is found to be infinite.

1.2 The Theory of Supersymmetry

One popular extension to the Standard Model is the theory of Supersymmetry (SUSY). A supersymmetric model of nature includes all of the SM particles plus a *superpartner* for each of them. Superpartners differ from their SM counterparts by spin $\frac{1}{2}$. Therefore, a SM fermion has a superpartner that is a boson (spin 0) and vice versa. If the differences were to stop there, the symmetry would be perfect. However this is not the case; the masses of the superpartners are different and the symmetry is said to be broken. The masses of the superpartners must be much larger than the SM particles (assuming they exist) because we have not been able to produce and observe them in present day colliders.

Supersymmetry is an attractive addition to the SM because of two reasons. First, the addition of the couplings of the superpartners to the Higgs boson cancels the diverging integral in the calculation of the Higgs mass [1]. Second, all of the forces become one at a very high interaction energy ($\sim 10^{14}$ GeV).

Physicists have always hoped that nature is very simple at the fundamental level. If SUSY exists in nature, then the strengths of the interactions, represented by the coupling constants, all become equal at this high energy. The forces are then indistinguishable and are considered to be unified. In the mid 1980's, the electromagnetic and weak forces were shown to be two manifestations of one force—the electroweak force.

In the model of Supersymmetry that our group is studying, there is a quantity known as R-parity. R-parity is defined in equation 1.1 (B is the baryon number ($B = \pm 1/3$ for quarks), L is the lepton number ($L = \pm 1$ for leptons), and S is the spin quantum number. It can be shown that all SM particles have $R = +1$ and all SUSY particles have $R = -1$.

$$R \equiv (-1)^{3B+L+2S} \tag{1.1}$$

For all interactions, the R-parity of the initial state must equal the R-parity of the final state. Therefore, one consequence of R-parity conservation is that a SUSY particle cannot decay into only SM particles—there exists a *lightest supersymmetric particle.*[2] This lightest SUSY particle is referred to as the neutralino and is written $\tilde{\chi}_1^0$.

Neutralinos interact only very weakly with matter (like neutrinos) and are not directly detectable. Because all of the heavier supersymmetric particles will decay into the $\tilde{\chi}_1^0$ before reaching the detector, a supersymmetric event will be signaled by missing energy. Thus good energy resolution is essential to the search for Supersymmetry.

---

[2] The stable particle must be the least massive because of conservation of energy in the rest frame of the parent particle. That is to say that a particle may not decay into particles of greater mass.

2 Studying Particles and Their Interactions

Physicists study particles by creating them in particle colliders and recording the information they leave when interacting with the detector. Europe, Japan and the United States have agreed to collaborate on the research and development of the Next Linear Collider (NLC).

A particle accelerator and a particle detector work together to produce the data to be studied. The NLC will accelerate electrons and positrons (anti-electrons) to very high energies and bring them together where annihilations create many other particles. Almost completely surrounding the interaction point is the cylindrically symmetric particle detector.

2.1 The Accelerator

The accelerator to be used in the NLC is being designed to create beams of electrons and positrons, accelerate them to an energy of 250 GeV while keeping the beam density high and to focus them to a very small cross section at the interaction point. Injectors, damping rings, main linear accelerators (linacs) and beam delivery systems work together to accomplish these goals.

Overall, the collider will be approximately 30 km long and 1 km wide. The injectors, damping rings and linacs are modeled directly after the ones used at the Stanford Linear Accelerator Center [2]. Damping rings use synchrotron radiation to reduce components of the velocity transverse to the beam. Beam delivery is accomplished in several stages: collimation, final focus, beam extraction and dump, etc.

2.2 The Detector

Detecting particles is done by recording what happens to materials as charged particles move through them. Detectors are made of several parts, including a vertex detector, drift chamber and calorimeter. As stated earlier, my study focuses on the calorimeter (a calorimeter is that which measures energy).

As shown in Figure 1, the calorimeter makes up the bulk of the detector. Electrons and positrons enter the detector through the beam line from opposite directions. When the electrons come close to one another in the middle of the detector they interact and sometimes annihilate. These interactions and annihilations produce other particles which travel radially outward.

Particles that are produced travel through the many parts of the detector leaving behind various types of signals for us to study. The electromagnetic calorimeter is primarily for detecting electrons, positrons, and photons. Outside of the ECAL is the hadron calorimeter which is used for detecting the energy of the hadrons.[3]

The concentric layers of the cylindrically symmetric calorimeters alternate between sensitive and non-sensitive materials. A sensitive material is one that produces a measurable signal when a charged particle deposits energy in it. Silicon and scintillator are the sensitive materials for the ECAL and HCAL, respectively. Tungsten and copper are the less costly non-sensitive materials in the ECAL and HCAL, respectively.

Silicon is a semiconductor which means that it will not conduct unless an electron is excited to a higher energy level (a *conduction band*) or the atoms are ionized. When charged particles pass through the layers of silicon in the ECAL, they interact with the atomic electrons and often ionize the atoms. A potential difference applied across the layer causes these electrons to move and it is this current which is detected. Charged particles passing though scintillator also ionize the atoms. However, the signal detected is light. Knock-on electrons (i.e. ionized electrons) in the scintillator leave *electron holes* that may be filled by more energetic electrons. When more energetic electrons drop down to the lower energy level (the electron hole), the energy lost manifests itself as a photon. These photons are detected by photomultipliers at the ends of the scintillator layers. These processes in the silicon and the scintillator also work when the atoms are simply excited (i.e. all the electrons stay bound, but one is pushed to a higher energy level).

Particles interact with the detector in various ways. The more important interactions are described below.

When photons interact with a material via the coulomb force, they produce an electron/positron pair.[4] The electron produced will loose energy by bremsstrahlung processes until its energy is about 10 MeV at which point it will be detected by ionization as described above [4]. Bremsstrahlung means "braking radiation" in German and is the name given to the emission of photons due to the acceleration of charged particles. The positron will loose energy by bremsstrahlung just like the electron until it is caught in a bound

---

[3] Hadrons are anything made of quarks, see Section 1.1.

[4] Photons may also loose energy by the photoelectric effect and Compton scattering. However, these processes only dominate at energies $\lesssim 20$ MeV [3].

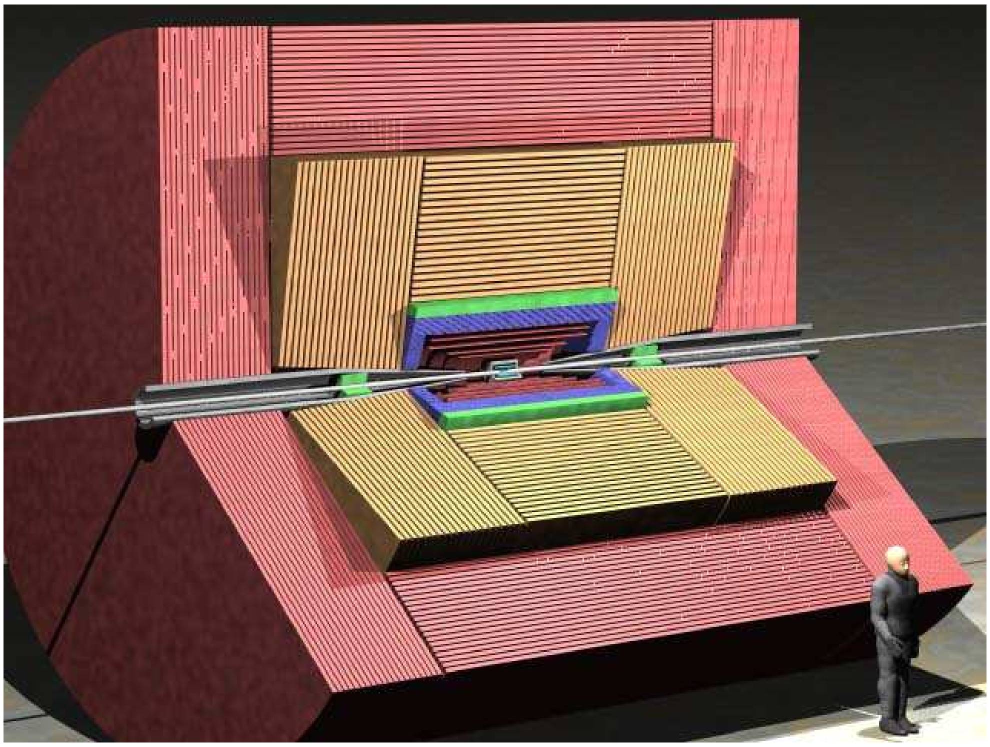

Figure 1: A rendition proposed particle detector to be used in conjunction with the next international linear collider. The yellow and blue layers are the hadronic and the electromagnetic calorimeters, respectively. The white line is the beam pipe, the outer red layer is the muon detector, the green layer between the calorimeters represents the magnet and the dark red inner layer is the drift chamber (these parts are not included in my simulation).

state with an atomic electron (the bound state is called positronium). Eventually, the electron and positron annihilate producing two or more photons. The bremsstrahlung photons go on to produce more electron-positron pairs and the process continues. This cascade of particles is called an electromagnetic shower.

Charged hadrons, when traveling through the scintillator, interact with the electrons in the atoms, knocking them out. This results in the emission and detection of photons as described above. Furthermore, all hadrons interact strongly with the nucleons[5] in the materials that make up the calorimeter. This means that the hadrons and nucleons will exchange gluons, some of which form quark-antiquark pairs. These new quarks and the quarks in the hadrons combine and recombine to form new hadrons. This process produces what is known as a *hadronic shower*. Characteristic of these hadronic showers are large angles between the velocities of the particles and less total energy detected than electromagnetic showers.

Neutral hadrons, like the neutron, are not directly detectable because they do not interact with electrons. The detection of neutral hadrons is dependent upon their strong interactions with other hadrons. When the hadrons interact strongly, some of their energy goes to the production of other hadrons just like charged hadrons. When these new hadrons are charged, they are detected. In this way, the energy of neutral hadrons is accounted for. Most hadrons are not stable—they decay into other hadrons. Nonetheless, the lifetimes are long enough that this is not something that needs to be considered in my study.

Muons do not create hadronic showers because they don't interact strongly. Muons, like all charged particles, emit photons when they are accelerated. However, the energy loss by this process is very small because the energy loss due to bremsstrahlung is inversely proportional to the mass squared. Muons are over 200 times as massive as electrons and have the same electric charge. Therefore, most of the time the only energy loss process undergone by muons is ionization. Muons are detected, but do not stopped by the detector; they carry energy away.

Neutrinos only interact weakly, consequently they do not shower like electrons and hadrons and they neither ionize nor excite atoms in the detector. Because of this, they pass through the detector, completely invisible, taking some of the energy with them.

---

[5] Nucleons are the constituents of the nucleus: protons and neutrons.

3 Computer Simulation

I have been working on a computer simulation of the detector mentioned above. My research is concerned with the energy resolution and the calibration of the detector.

GEANT is the name of the detector description and simulation software tool I use in my studies. I have written FORTRAN code that describes the detector geometry, initializes the events to be run and outputs the interesting data. I have also written Perl programs to run the simulation, save log files and keep track of the proper random number generator seeds. Copies of these files may be found on line at `http://hep-www.colorado.edu/~duckwitz/`.

Data is output to an ASCII file. Included in the information that is saved every event is the initial particle's ID, incident energy and energy deposited in both the ECAL and HCAL. These data files are compressed in a format called an ntuple and analyzed using Physics Analysis Workstation (PAW).

The detector geometry I have simulated is called the Small detector and its parameters are shown in Table 3. There is an alternative geometry called the Large detector and it is being studied by another member of our research group. There are a couple of differences between my simulation and the actual Small detector design. First, my simulation does not include the magnet material. Note that this is true even in the simulations with the magnetic field. Second, the ECAL has only tungsten and silicon layers; while, in the actual design, there will be layers of air and G10 (which is a mixture of silicon-dioxide and epoxy). It is our guess that the absence of the air and G10 layers makes little difference, though we have done no simulations to show this.

I simulated the two calorimeters separately and the number of layers in each calorimeter was made infinite. For simulation purposes, an infinite calorimeter means that the number of layers was large enough so that all the energy incident on the calorimeter would be deposited. Particles carrying away energy by escaping from the detector is called *punch-through*). Hadrons inevitably have a fair amount of missing energy due to neutrino production, $\approx 30\%$ lost.

Over 4 million events have been simulated using different particles, particle trajectories and incident energies. The data is used to find the energy resolution as a function of the initial particle energy and angle and the calibration of the detector as described in the following sections.

Data was obtained for calorimeters with and without a magnetic field.

Section	Parameter	Value
Hadronic Barrel	Number of Layers	38
	Copper Thickness	2.0cm
	Scintillator Thickness	0.5cm
	Inner Radius	140cm
	Length	265cm
Hadronic Endcaps	Number of Layers	38
	Copper Thickness	2.0cm
	Scintillator Thickness	0.5cm
	Inner Radius	20cm
EM Barrel	Number of Layers	50
	Tungsten Thickness	0.2cm
	Silicon Thickness	0.03cm
	Inner Radius	75cm
	Length	155cm
EM Endcaps	Number of Layers	50
	Tungsten Thickness	0.2cm
	Silicon Thickness	0.03cm
	Inner Radius	20cm

Table 3: Small detector geometry parameters.

I simulated 10,000 electrons and pions in both the ECAL and the HCAL with energies of 2, 3, 4, 6, 8, 10, 15, 20, 30, 40 and 50 GeV[6] and at polar angles, $\theta = 90$, 60, 45, 30 and 20 degrees. Because the endcaps have the same layer thicknesses as the barrels and because of the layer orientations, the particles entering the barrel interact with the detector in much the same way as in the endcaps (see Fig. 2). Therefore, we expect that the resolution for $\theta = 90^\circ - \phi$ to be the same as the resolutions for $\theta = \phi$, for ϕ between 10° and 40° when there is no magnetic field. Comparing data for $\theta = 60$ and $\theta = 30$ (corresponding to $\phi = 30$) I found that the difference in resolutions was on the order of my statistical error ($\approx 3\%$). When the magnetic field was used in the simulation, these resolutions were, as expected, different.

Ideally the detectors would be made completely of sensitive material. Because this is expensive, cheaper materials are used (lead, tungsten or copper). By alternating layers of sensitive and cheaper materials we find the maximum effectiveness with the minimum cost.

---

[6] An electron-volt (eV) is defined as the energy gained by a particle with the charge of an electron moving through a potential difference of one volt. 1 GeV = 10^9 eV.

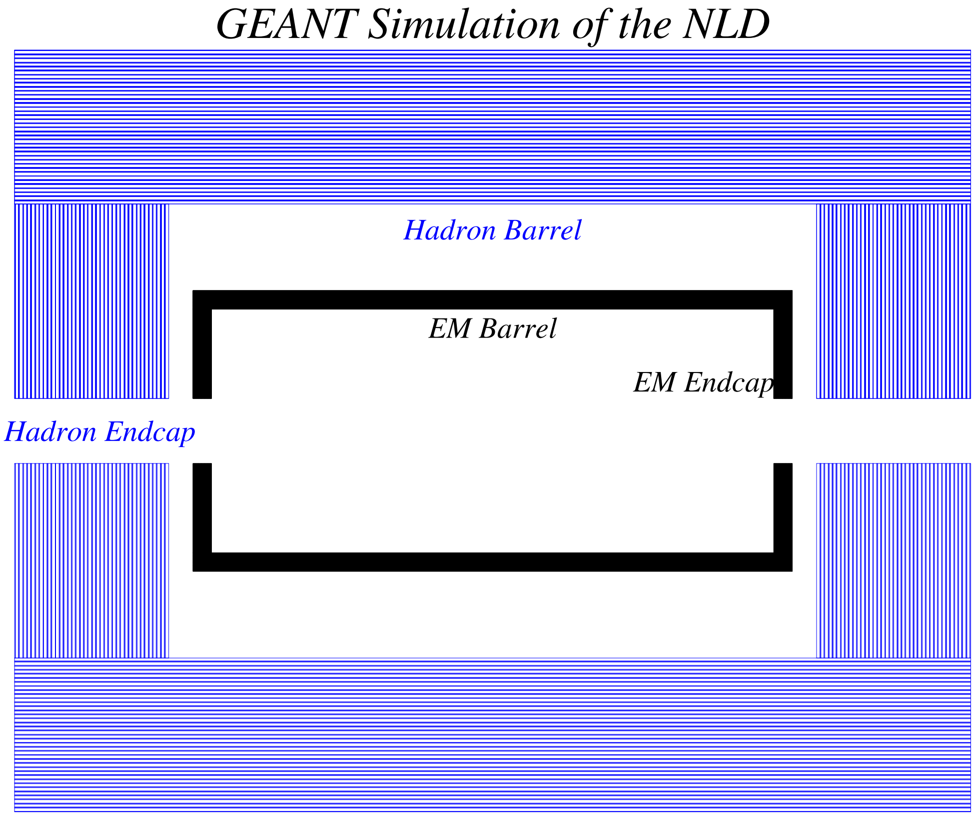

Figure 2: Cross sectional view of the detector (xz-plane) drawn by GEANT. The particle beams enter from the left and right.

4 Energy Resolution

As stated before, the energy resolution of the detector is important in the search for Supersymmetry. Section 2.2 described how the energy of particles is detected. Not all of the energy deposited is detected[7] and particles with the same initial energy don't always deposit the same amount of energy due to statistical fluctuations. An example energy distribution is shown in Figure 3.

Theory predicts that the error in the energy divided by the energy is linear in the inverse square root of the incident energy as follows (see Appendix A):

$$\frac{\delta E_{dep}}{E_{dep}} \equiv \frac{\sigma}{\mu} = a + \frac{b}{\sqrt{E}} \tag{4.1}$$

where E_{dep} is the energy deposited in the sensitive layers of the calorimeter, a is the intercept, b is the slope, σ and μ are the standard deviation and mean (respectively) of the distribution of deposited energies and E is the incident energy. This quantity, $\frac{\delta E_{dep}}{E_{dep}}$, is defined to be the resolution of the detector. Finding the slope and intercept required using the line of best fit of σ/μ versus $1/\sqrt{E}$. Appendix B shows how I obtained the errors on the slope and resolution.

There was one difference between analyzing the electron and pion data. The electron data sets were fit to a gaussian and pion data sets were fit to a double gaussian (the sum of two gaussians). Pions produce a high energy tail which makes the distribution deviate from a gaussian. A second gaussian is added to account for this tail. The mean and standard deviation used were taken from the gaussian that takes into account most of the data (the major gaussian). Figure 4 shows a typical data distribution for pions. Notice the high energy tail which is not present in the electron data, Figure 5.

The probability distribution for ionization energy loss is given by the Landau distribution [3]. Figure 6 and equation 4.2 characterize the general shape of the Landau distribution, $L(\lambda)$, where λ is an arbitrary parameter. The total energy deposited is the sum over these energy losses via ionization and therefore we expect to observe this high energy tail in the pion data. Also contributing the the high energy tail is the occasional production of an electron or photon and thus an electromagnetic shower. More energy is detected in electromagnetic showers than in hadronic showers as mentioned

---

[7] In fact, the amount of energy detected is around 2% of the total energy of the particle.

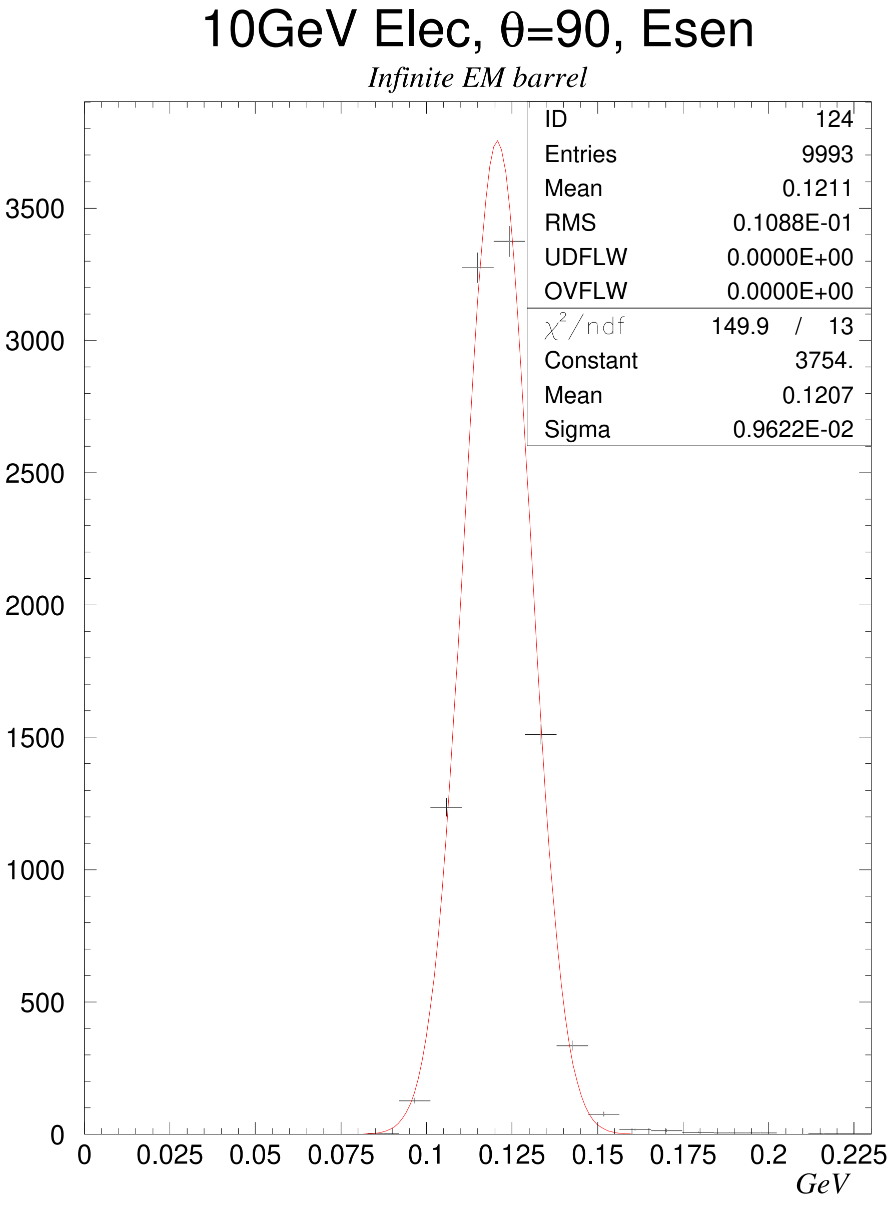

Figure 3: Distribution of the energy deposited by 10,000 electrons with 10 GeV of initial energy in an infinite electromagnetic barrel.

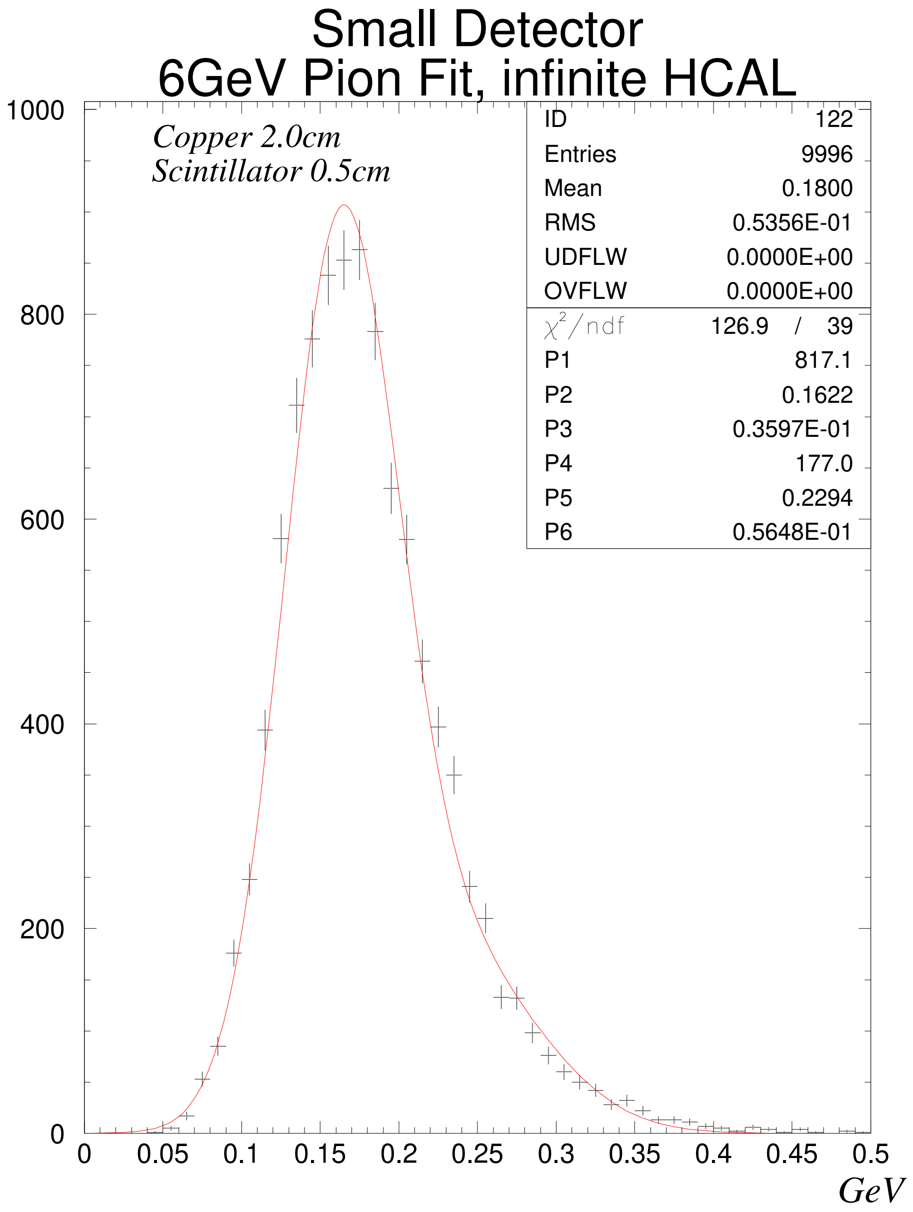

Figure 4: Typical energy distribution histogram with a double gaussian fit. Pions with an incident energy of 6 GeV were simulated and the energy deposited in the sensitive layers of the calorimeter is plotted.

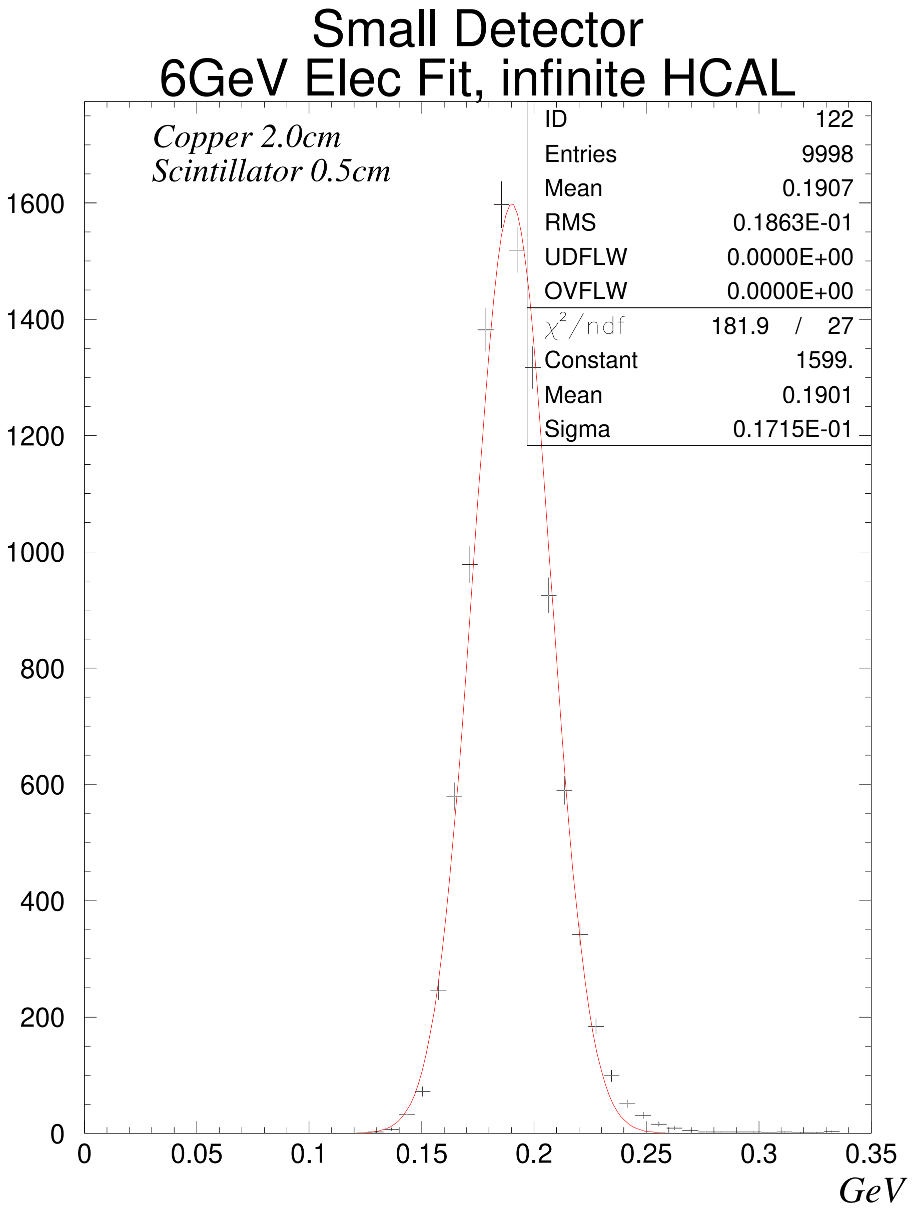

Figure 5: Typical energy distribution histogram with a gaussian fit. Electrons with an incident energy of 6 GeV were simulated and the energy deposited in the sensitive layers of the calorimeter is plotted.

in Section 2.2.

$$L(\lambda) = \frac{1}{\sqrt{2\pi}} e^{-\frac{1}{2}\left(\lambda + e^{-\lambda}\right)} \tag{4.2}$$

High energy tails are not observed in the electron data because electrons deposit energy by ionization many more times than pions in a single shower. The Central Limit Theorem states that the distribution of the sum of data points approaches a gaussian as the number of data points gets large [5]. Pions with a large incident energy ($\gtrsim$ 20 GeV) deposit energy via ionization a larger number of times than low energy pions and thus produce energy distributions that are more gaussian as seen in Figure 7.

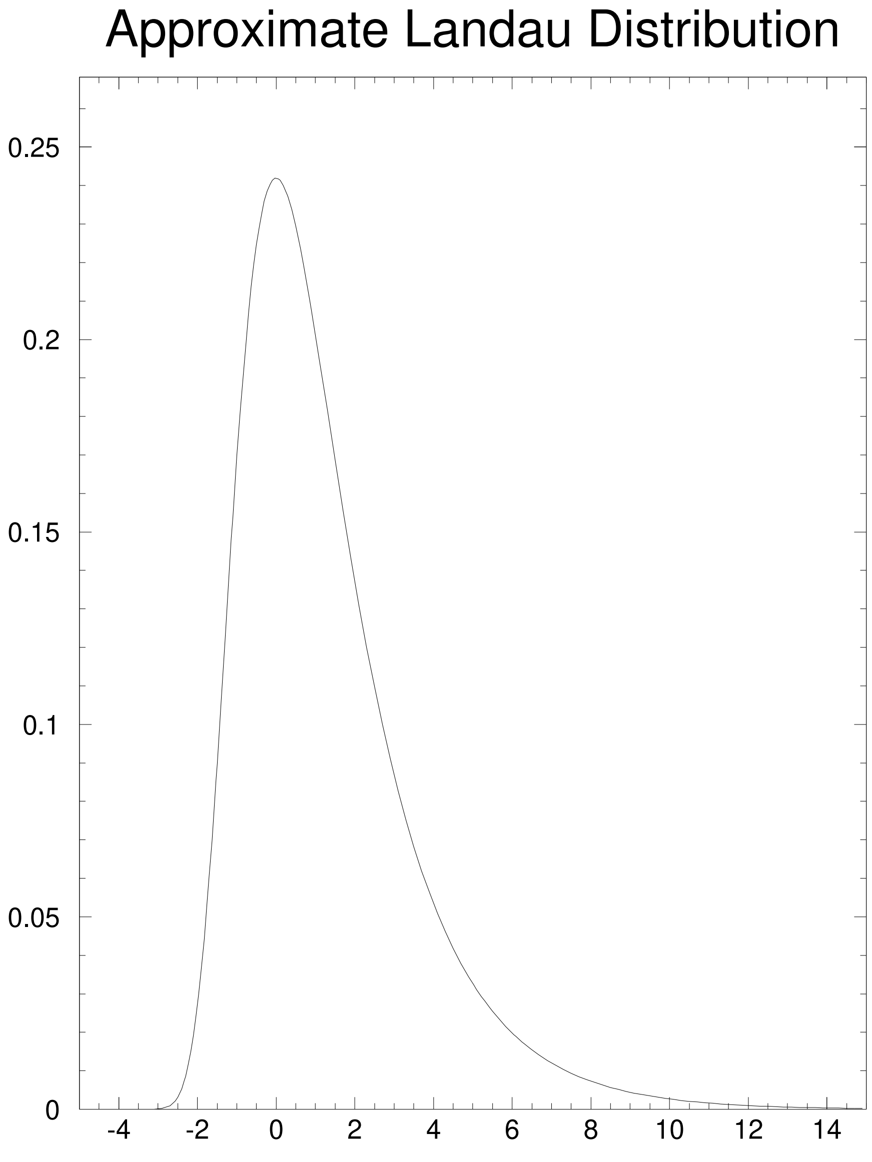

Figure 6: A plot of the approximate Landau distribution, equation 4.2. Compare the shape of this plot with Figure 4 on page 14.

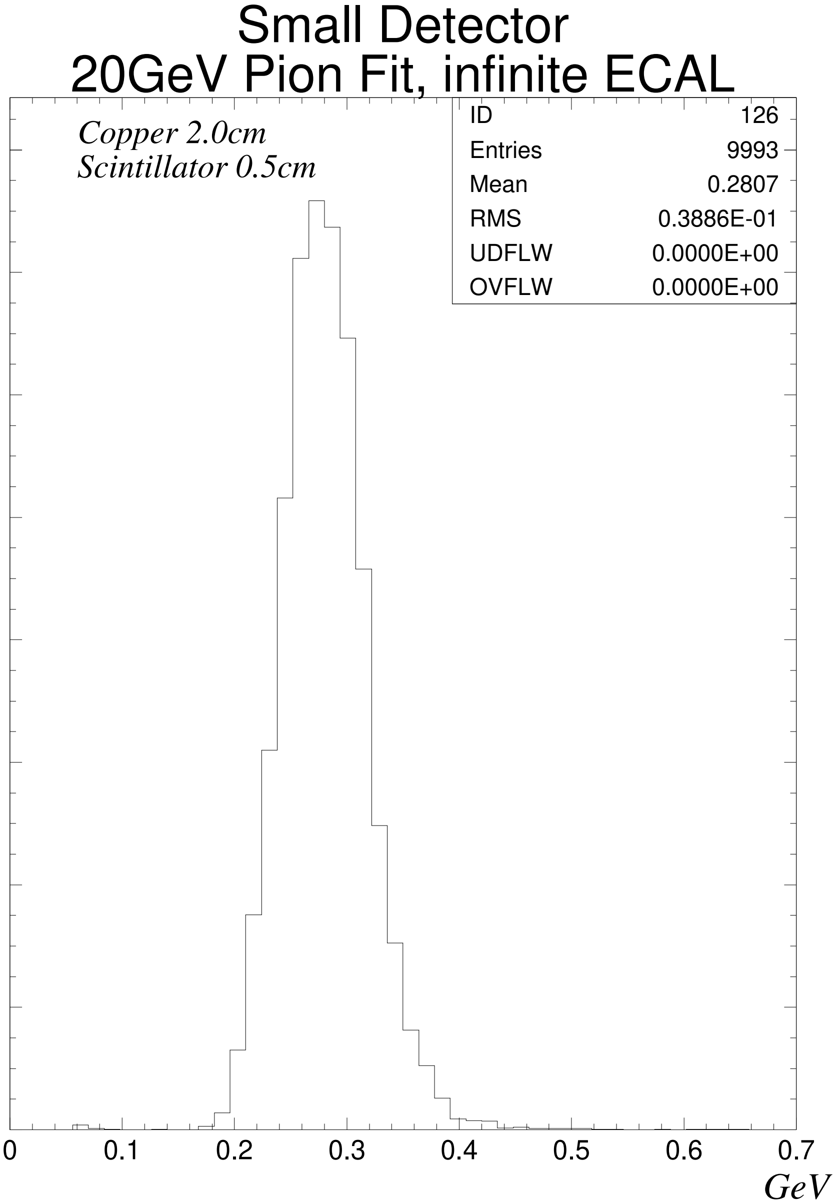

Figure 7: Distribution of energy deposited by 10,000 pions initially with an energy of 20 GeV.

Particle	Calorimeter	θ	Intercept	Slope
Electrons	ECAL	90	0.0090 ± 0.0004	0.167 ± 0.001
Electrons	HCAL	90	0.0066 ± 0.0003	0.2012 ± 0.0009
Electrons	ECAL	60	0.0089 ± 0.0004	0.171 ± 0.001
Electrons	HCAL	60	0.0063 ± 0.0007	0.220 ± 0.002
Electrons	ECAL	45	0.0083 ± 0.0005	0.182 ± 0.002
Electrons	HCAL	45	0.0045 ± 0.0007	0.249 ± 0.002
Electrons	ECAL	30	0.0089 ± 0.0004	0.171 ± 0.001
Pions	ECAL	90	0.038 ± 0.004	0.37 ± 0.02
Pions	HCAL	90	0.016 ± 0.003	0.49 ± 0.01
Pions	ECAL	60	0.031 ± 0.003	0.39 ± 0.01
Pions	HCAL	60	0.013 ± 0.005	0.50 ± 0.02
Pions	ECAL	45	0.031 ± 0.003	0.39 ± 0.01
Pions	HCAL	45	0.011 ± 0.007	0.53 ± 0.03
Pions	HCAL	30	0.010 ± 0.001	0.519 ± 0.003

Table 4: Slope and intercept summary for the Small detector resolution in infinite calorimeters with no magnetic field.

4.1 No Magnetic Field

The resolutions are summarized in Table 4. Also, examples of the resolution fits for the Small detector are shown in Figures 8-11.[8] Some of the resolution plots (e.g. Fig. 10) reveal that the resolution of particles of incident energies $\lesssim 2$ GeV is worse than at larger energies. Because of this, I have fit two lines to several of the data sets. One fit includes all incident energies (blue line) and one excludes the 2 GeV point (red line).

---

[8] All of the resolution fits may be found on the World Wide Web at `http://hep-www.colorado.edu/SUSY/`.

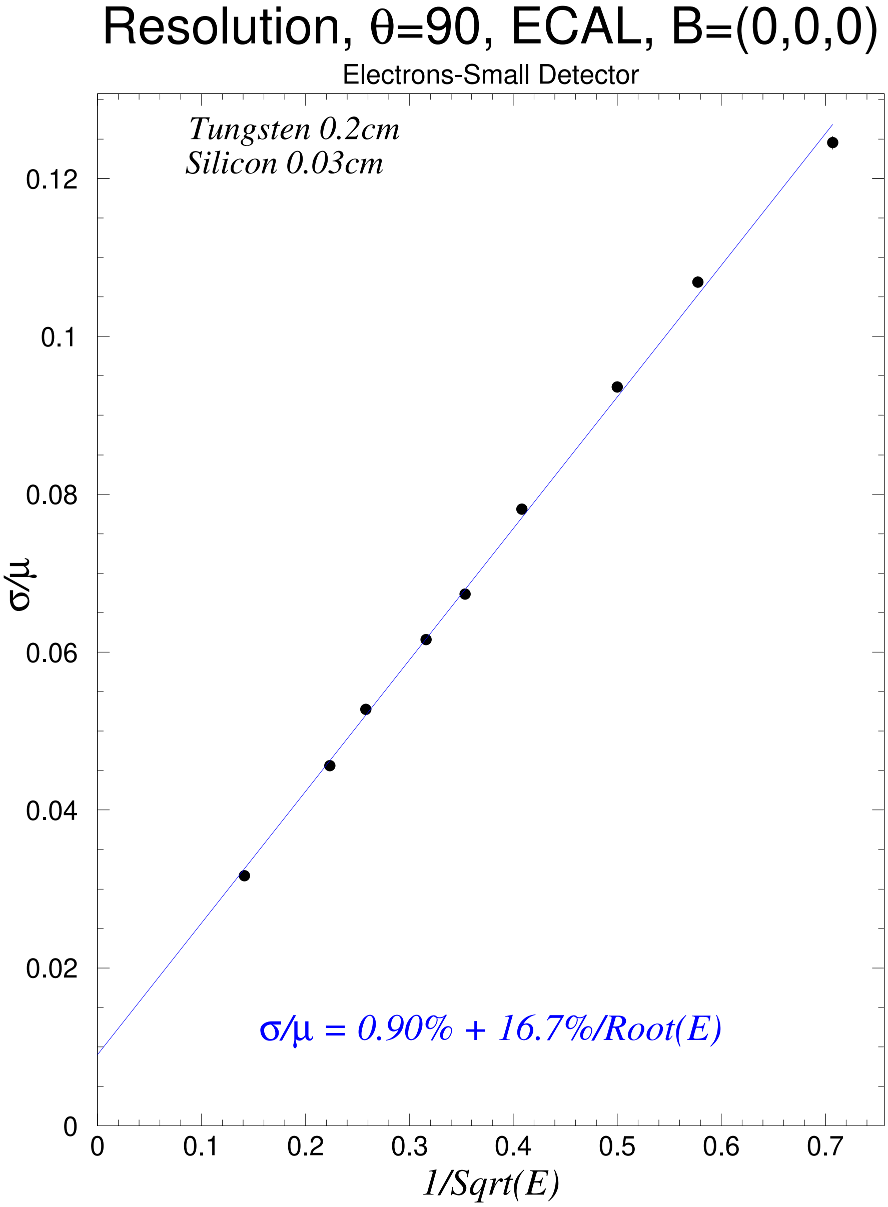

Figure 8: Small detector resolution of the ECAL for electrons at a polar angle equal to 90 degrees with no magnetic field.

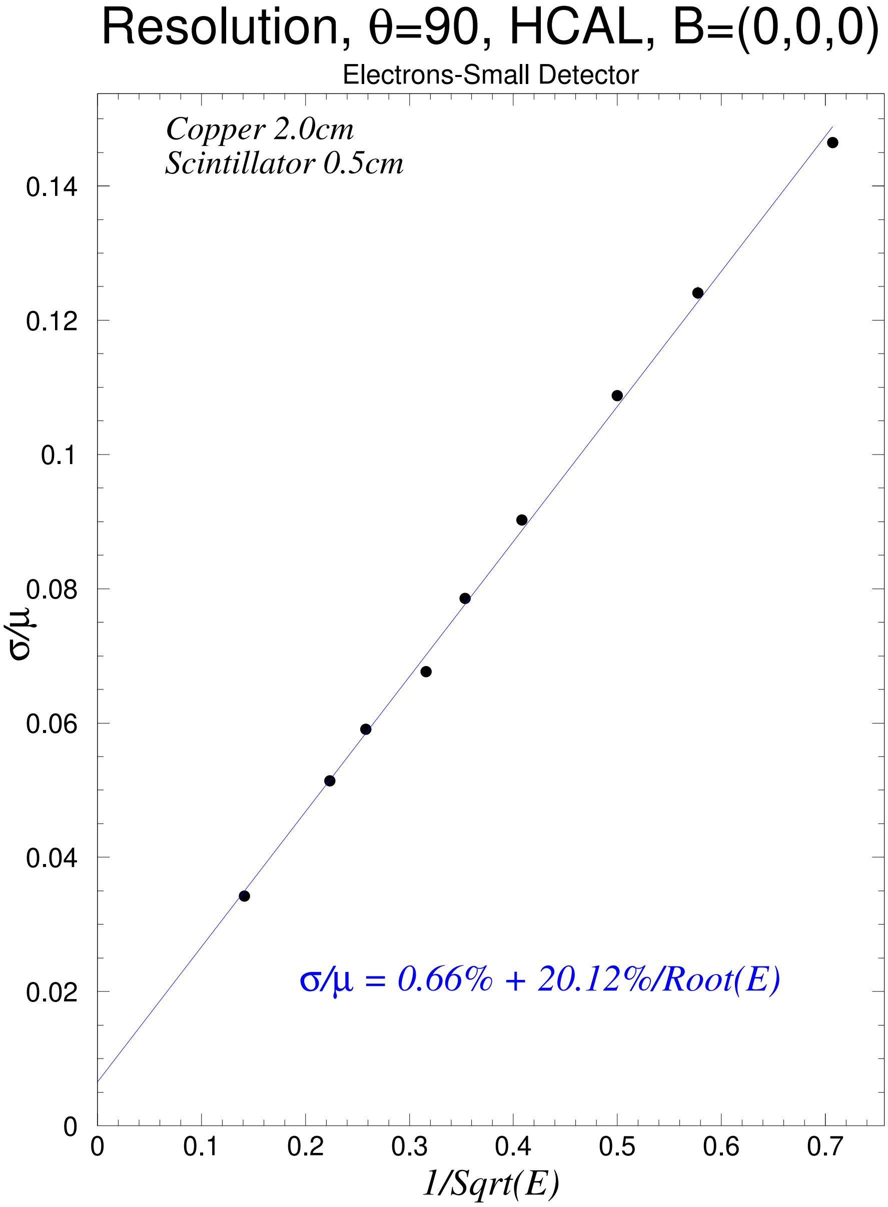

Figure 9: Small detector resolution of the HCAL for electrons at a polar angle equal to 90 degrees with no magnetic field.

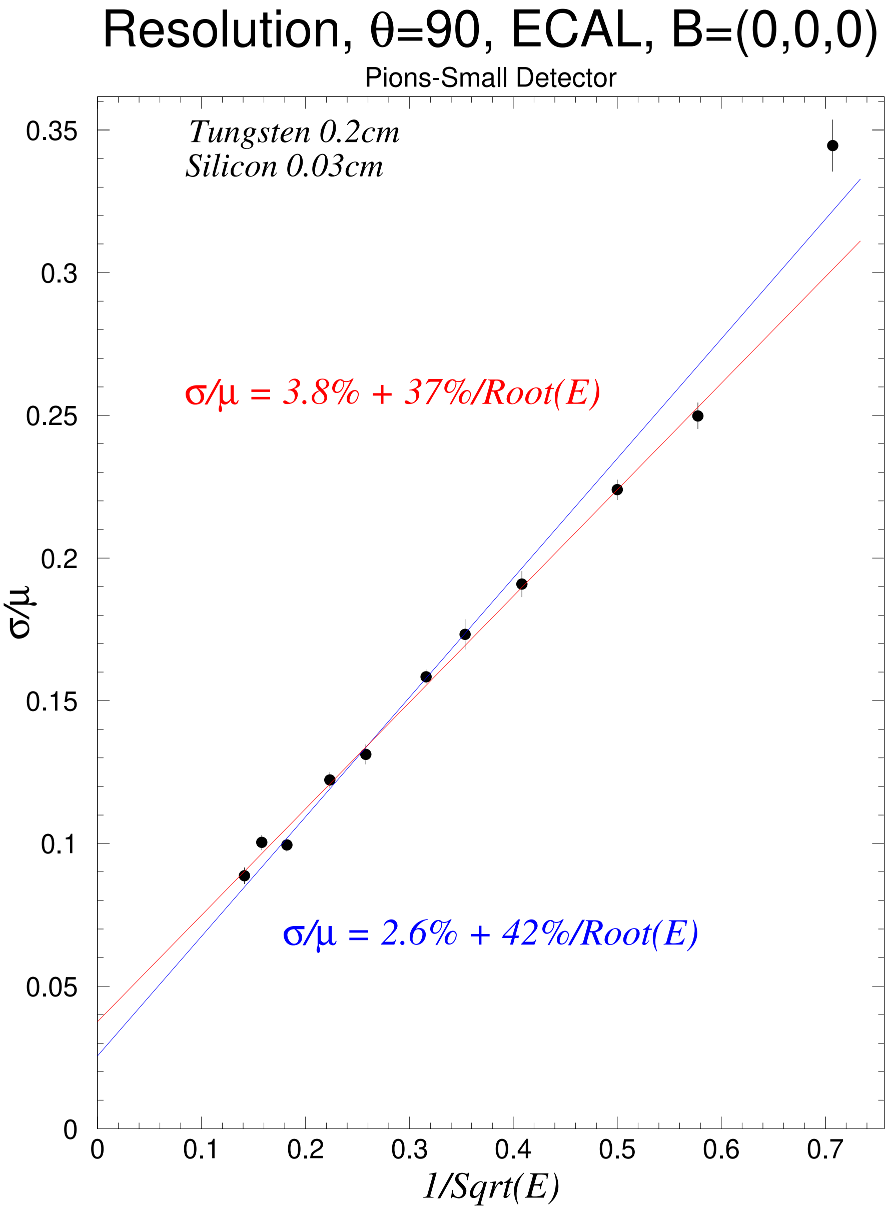

Figure 10: Small detector resolution of the ECAL for pions at a polar angle equal to 90 degrees with no magnetic field.

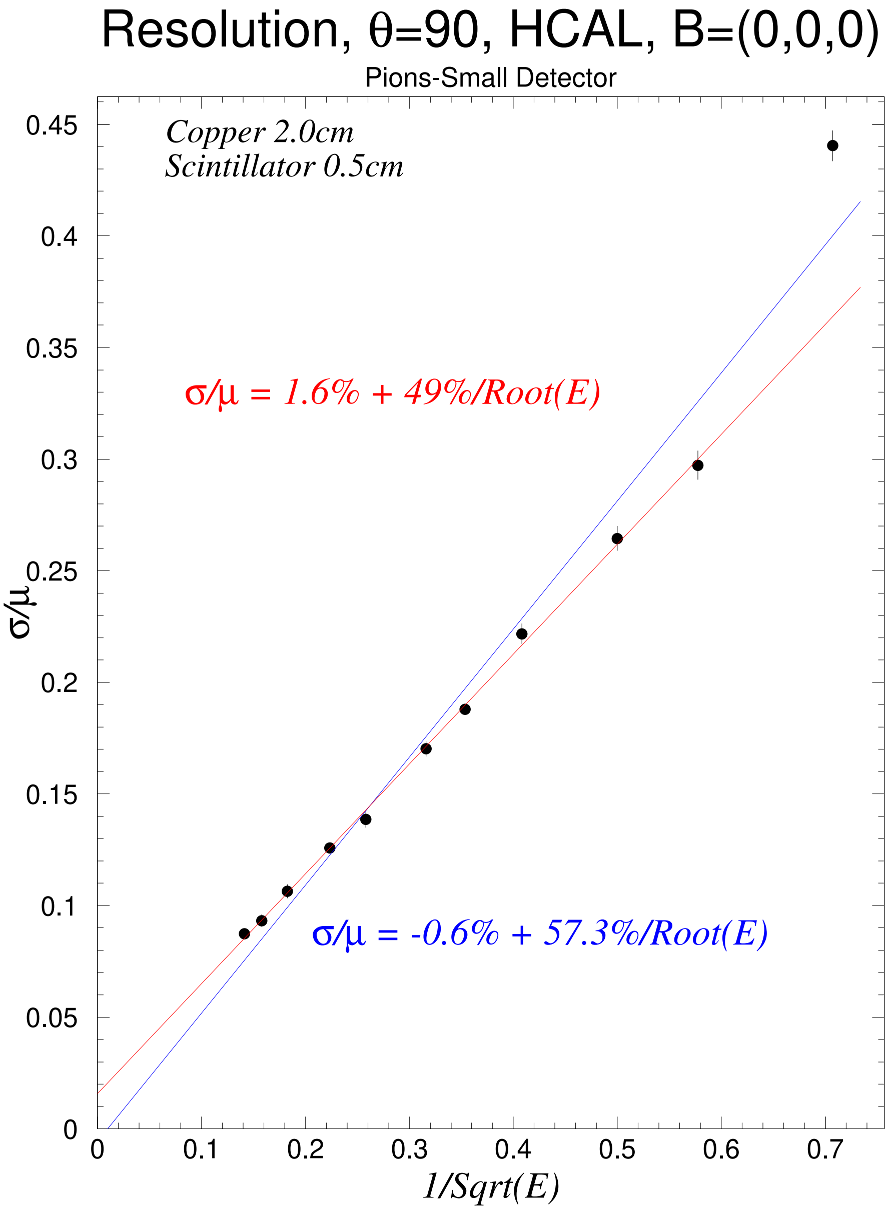

Figure 11: Small detector resolution of the HCAL for pions at a polar angle equal to 90 degrees with no magnetic field.

Particle	Calorimeter	θ	Intercept	Slope
Electrons	ECAL	90	0.0075 ± 0.0004	0.169 ± 0.001
Electrons	HCAL	90	-0.0009 ± 0.0003	0.258 ± 0.002
Electrons	ECAL	60	0.0080 ± 0.0004	0.172 ± 0.001
Electrons	HCAL	60	0.0023 ± 0.0007	0.262 ± 0.003
Electrons	ECAL	45	0.0068 ± 0.0004	0.186 ± 0.001
Electrons	HCAL	45	0.0094 ± 0.0005	0.261 ± 0.001
Electrons	ECAL	30	0.0079 ± 0.0004	0.176 ± 0.001
Electrons	HCAL	30	0.0069 ± 0.0005	0.214 ± 0.002
Electrons	ECAL	20	0.0091 ± 0.0004	0.170 ± 0.001
Electrons	HCAL	20	0.0069 ± 0.0005	0.206 ± 0.002
Pions	ECAL	90	0.031 ± 0.003	0.39 ± 0.01
Pions	HCAL	90	0.015 ± 0.006	0.51 ± 0.01
Pions	ECAL	60	0.031 ± 0.002	0.39 ± 0.01
Pions	HCAL	60	0.017 ± 0.007	0.52 ± 0.03
Pions	ECAL	45	0.028 ± 0.003	0.39 ± 0.01
Pions	HCAL	45	0.021 ± 0.006	0.51 ± 0.03
Pions	ECAL	30	0.0301 ± 0.0016	0.388 ± 0.01
Pions	HCAL	30	0.014 ± 0.002	0.509 ± 0.03
Pions	ECAL	20	0.029 ± 0.001	0.407 ± 0.002
Pions	HCAL	20	0.013 ± 0.001	0.505 ± 0.003

Table 5: Slope and intercept summary for the Small detector resolution in infinite calorimeters with a magnetic field of 6 tesla.

4.2 Constant Magnetic Field

Resolutions with a 6 tesla magnetic field are shown in Table 5. I have included a set of resolution fits done with a magnetic field that is similar to that given in the previous section. Figures 12-15 show the resolution fits for electrons and pions in the HCAL and ECAL for $\theta = 90°$.

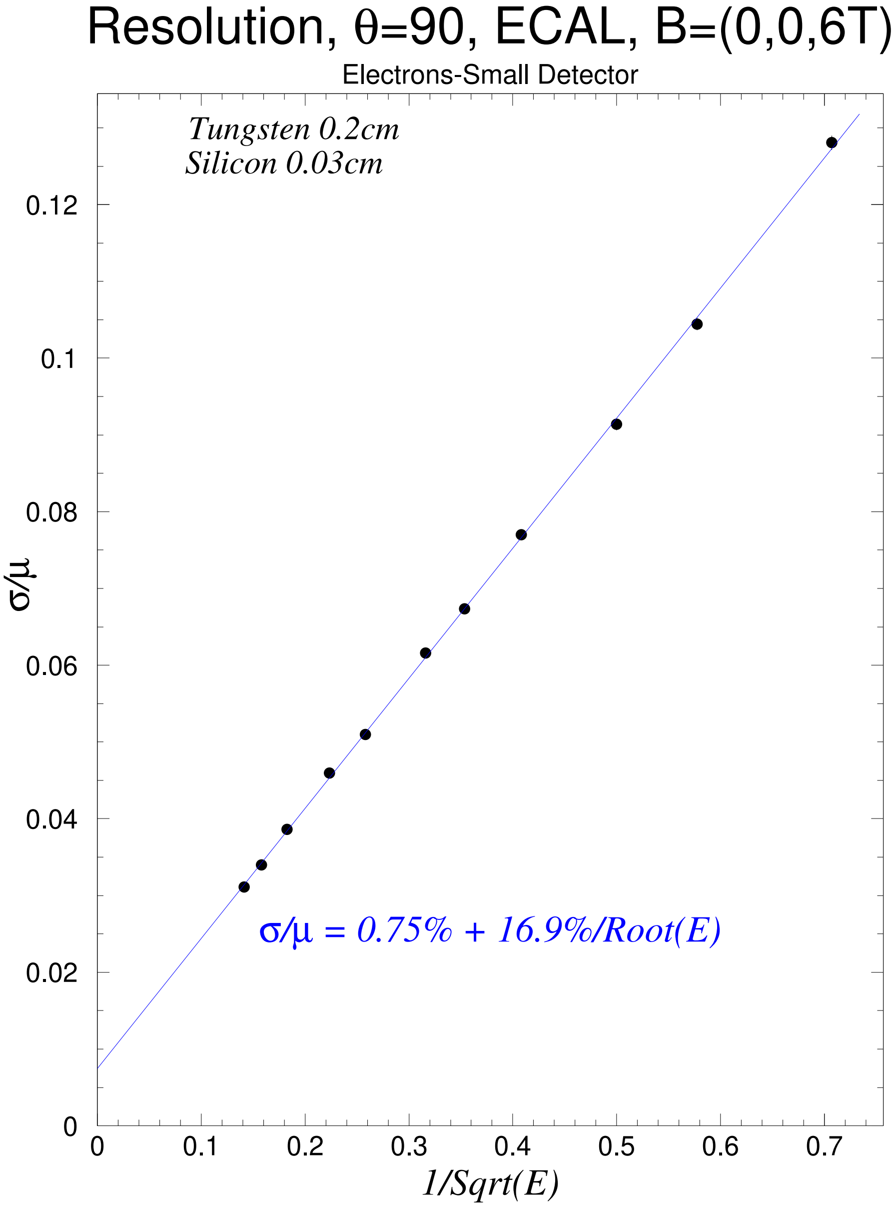

Figure 12: Small detector resolution of the ECAL for electrons at a polar angle equal to 90 degrees with a magnetic field of 6 tesla.

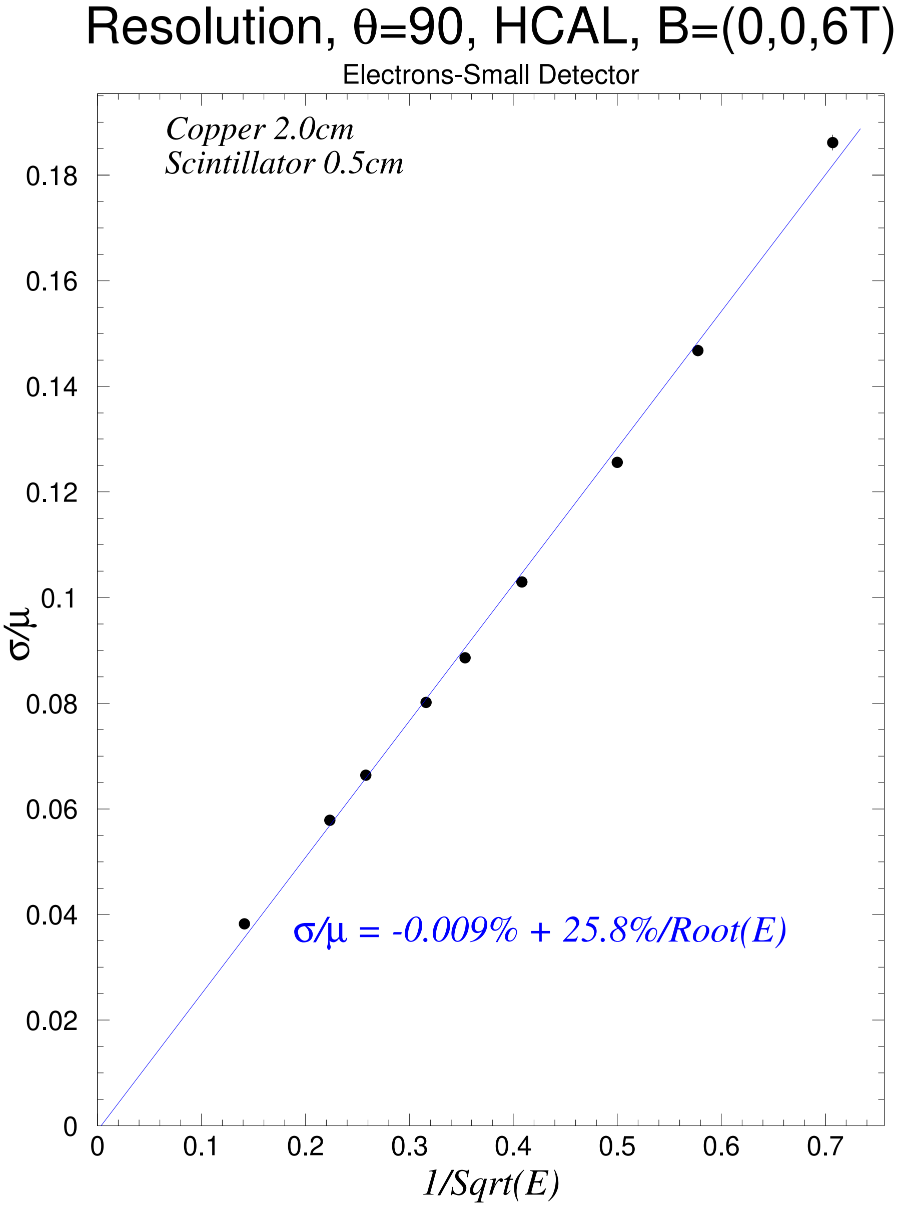

Figure 13: Small detector resolution of the HCAL for electrons at a polar angle equal to 90 degrees with a magnetic field of 6 tesla.

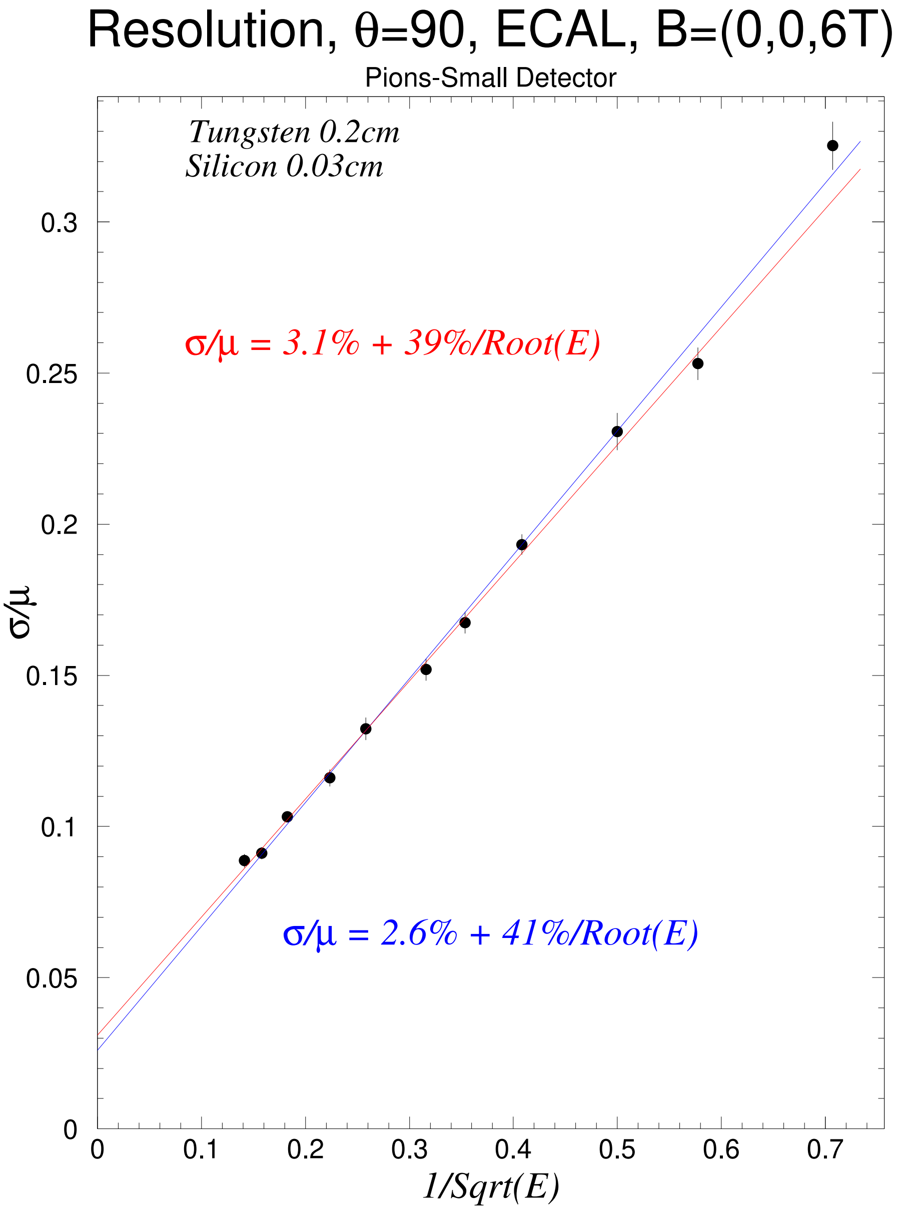

Figure 14: Small detector resolution of the ECAL for pions at a polar angle equal to 90 degrees with a magnetic field of 6 tesla.

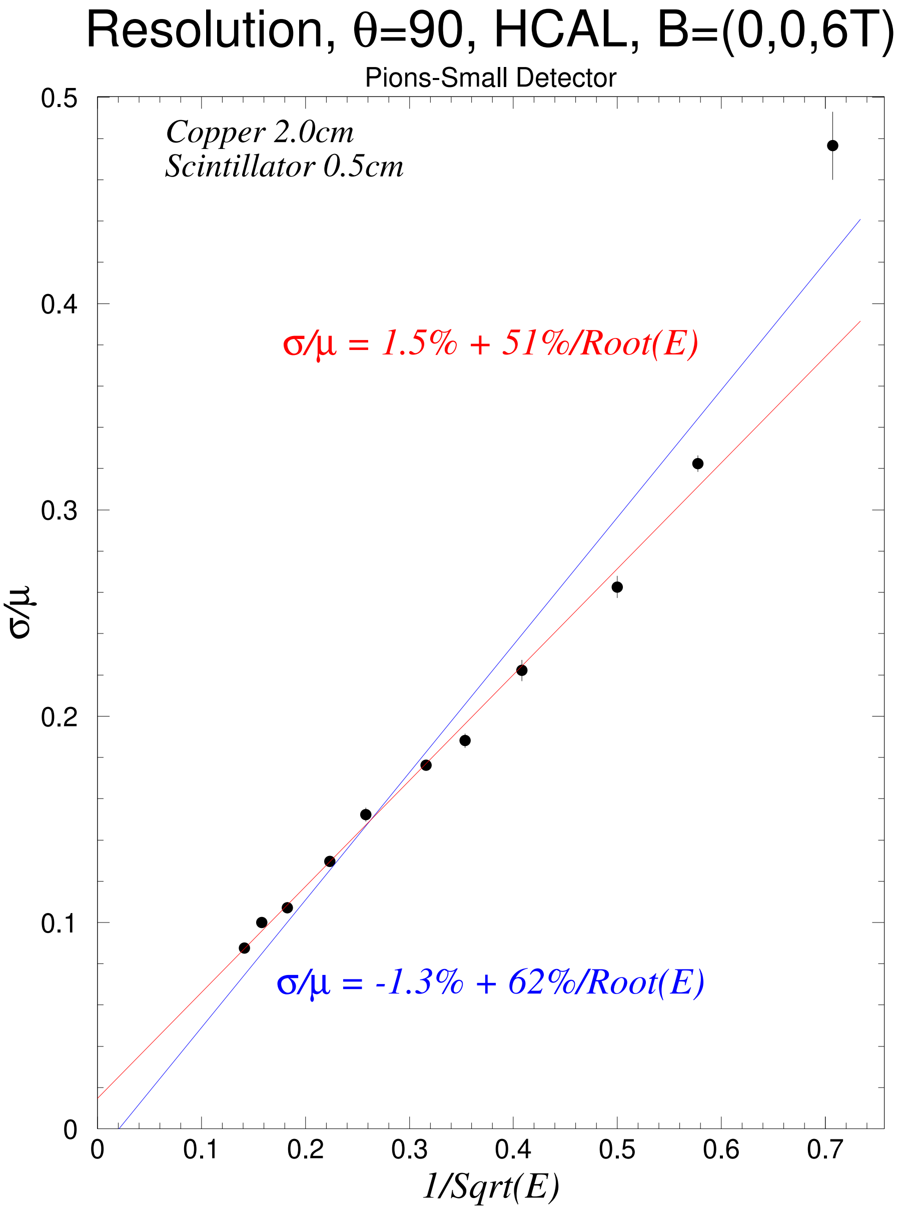

Figure 15: Small detector resolution of the HCAL for pions at a polar angle equal to 90 degrees with a magnetic field of 6 tesla.

5 Detector Calibration

The calibration of the detector is a method for determining the incident energy of particles given the amount of energy deposited in the sensitive layers (i.e. the energy observed). Particle tracks left in the detector before they reach the calorimeters will help identify particles (for example, drift chambers are used to find the charge to mass ratio). Once we know what type of particle interacted with the detector and how much energy it deposited in the sensitive layers, we can find its initial energy.

Using the data below, one will be able to infer the incident energy of the particle by linearly interpolating between the points in the tables. There is a one-to-one correspondence between the incident energy of the particle and the amount of its energy that is detected.

5.1 No Magnetic Field

Figures 16 and 17 show the energy detected as a function of incident energy. The data values are also in Tables 6-9. Plots of the ratio of the energy detected to the incident energy are displayed in Figures 18 and 19. Note that Figure 18 shows that the fraction of energy deposited drops drastically for pions with energy less than ≈ 10 GeV. The amount of energy deposited is not tabulated here because it may easily be calculated from the ratio of energy deposited to the incident energy.

Particle	Calorimeter	2 GeV	3 GeV	4 GeV	6 GeV	8 GeV	10 GeV
e^-	ECAL	0.0178	0.0179	0.0179	0.0179	0.0179	0.0179
e^-	HCAL	0.0314	0.0315	0.0316	0.0317	0.0318	0.0317
π	ECAL	0.0117	0.0127	0.0136	0.0139	0.0136	0.0138
π	HCAL	0.0209	0.0226	0.0248	0.0270	0.0270	0.0271

Particle	Calorimeter	15 GeV	20 GeV	30 GeV	40 GeV	50 GeV
e^-	ECAL	0.0180	0.0179	0.0180	0.0180	0.0180
e^-	HCAL	0.0318	0.0318	0.0319	0.0319	0.0319
π	ECAL	0.0141	0.0145	0.0147	0.0154	0.0157
π	HCAL	0.0280	0.0286	0.0292	0.0297	0.0302

Table 6: Ratios of the energy deposited in sensitive layers to the incident energy for $\theta = 90°$ and no magnetic field.

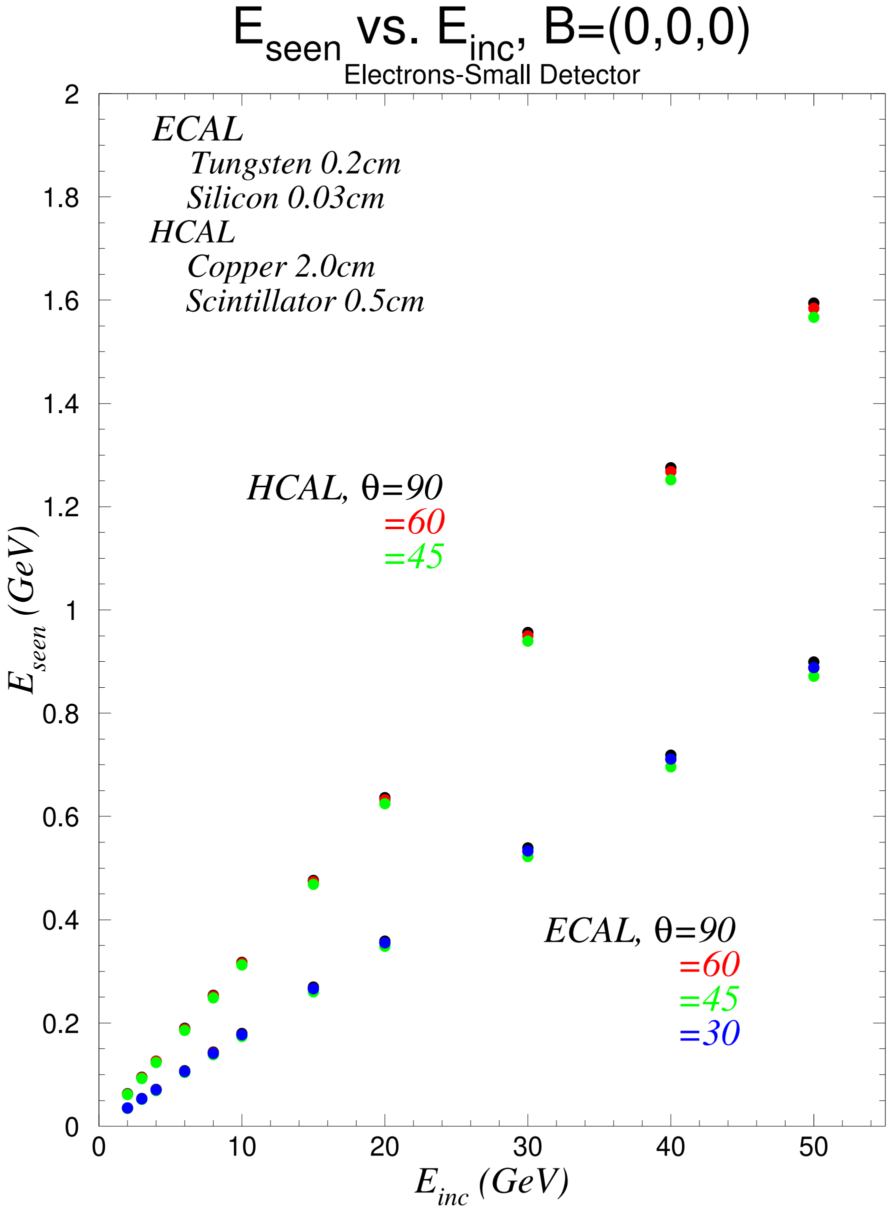

Figure 16: Energy detected by the sensitive layers with no magnetic field as a function of the incident energy of the electron.

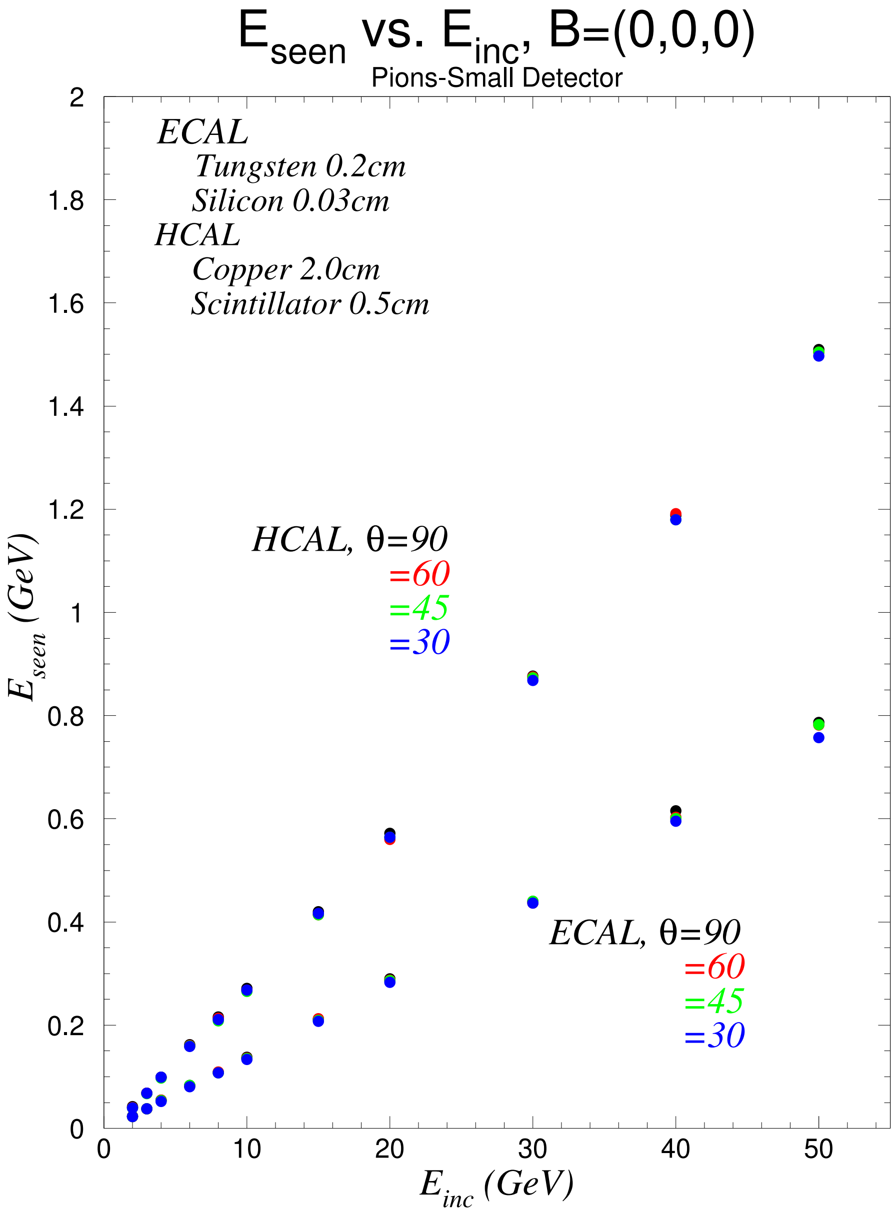

Figure 17: Energy detected by the sensitive layers with no magnetic field as a function of the incident energy of the pion.

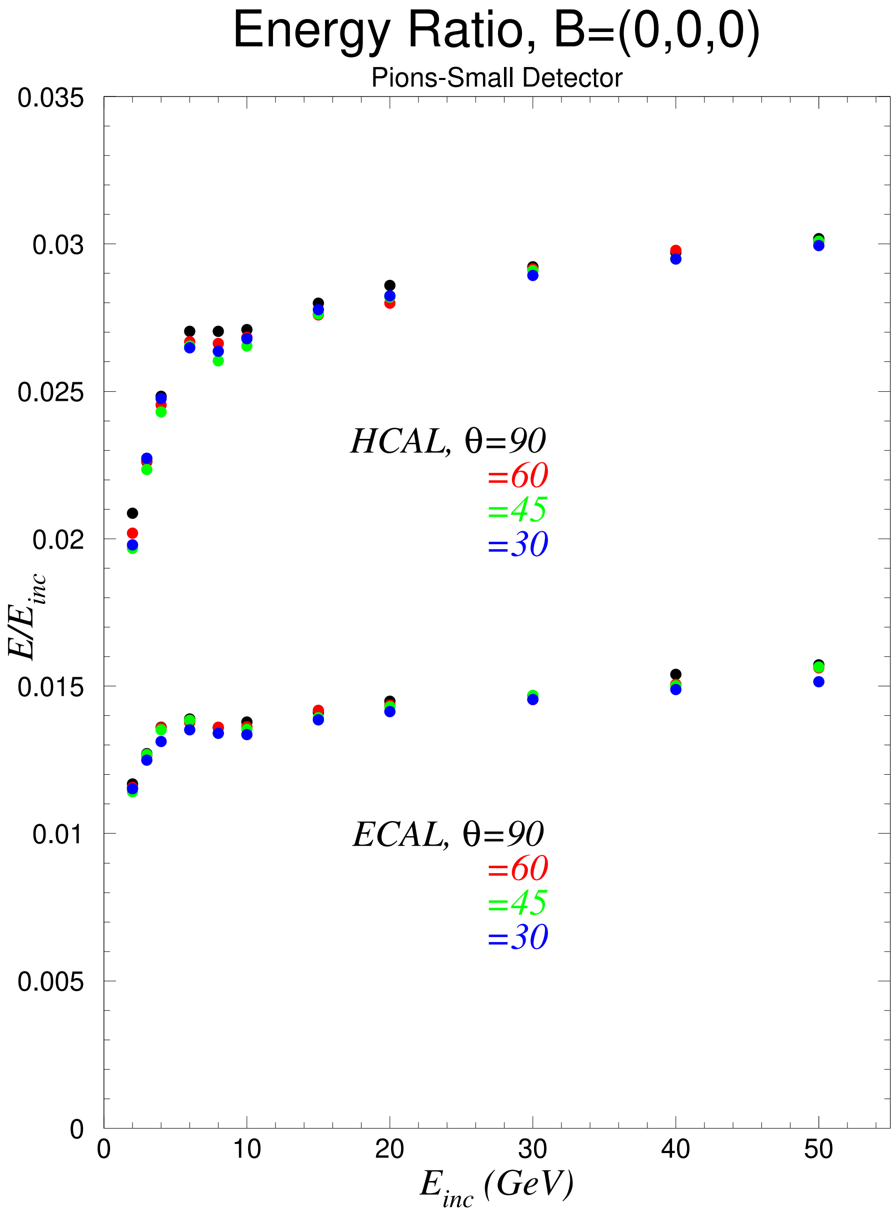

Figure 18: Ratio of the energy detected by the sensitive layers with no magnetic field to the incident energy of the pion.

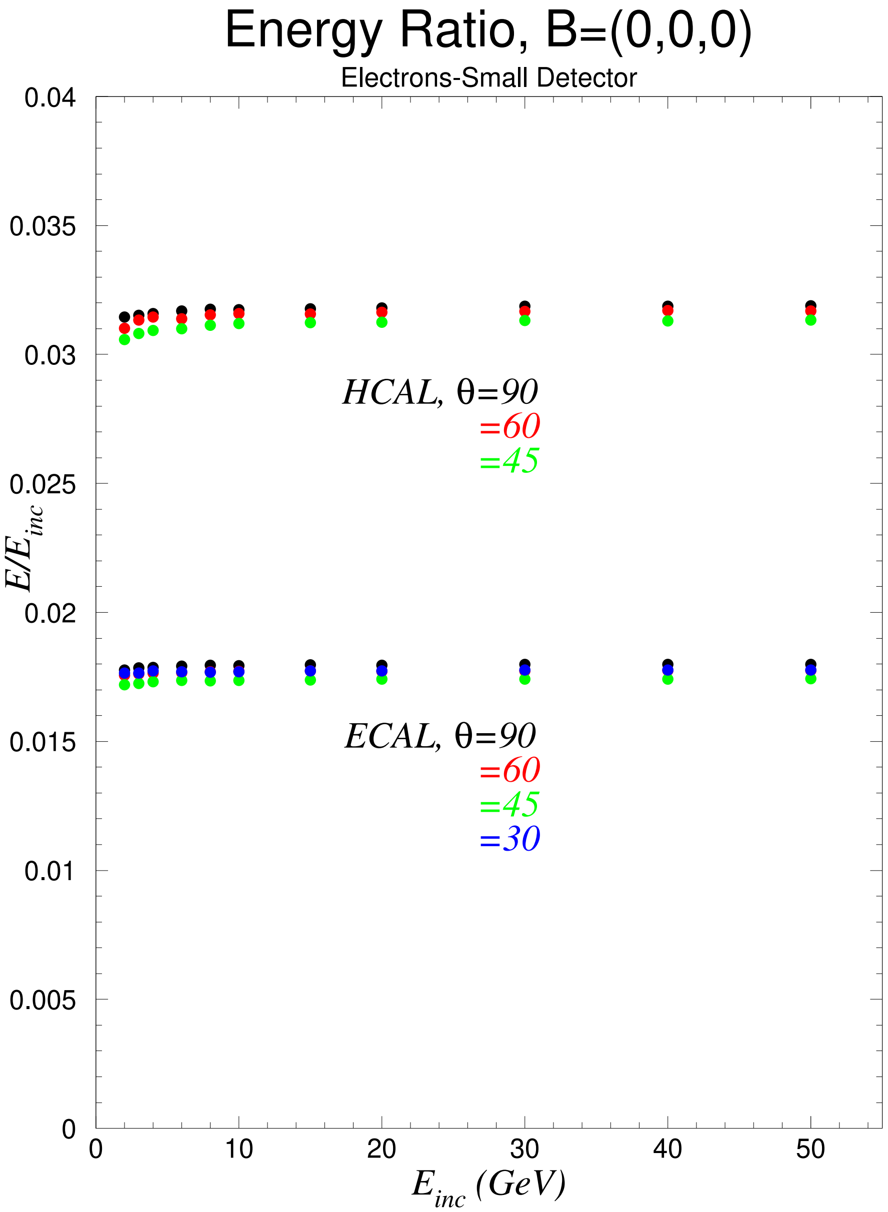

Figure 19: Ratio of the energy detected by the sensitive layers with no magnetic field to the incident energy of the electron.

Particle	Calorimeter	2 GeV	3 GeV	4 GeV	6 GeV	8 GeV	10 GeV	15 GeV	20 GeV	30 GeV	40 GeV	50 GeV
e^-	ECAL	0.0176	0.0176	0.0177	0.0177	0.0177	0.0177	0.0177	0.0177	0.0177	0.0178	0.0178
e^-	HCAL	0.0310	0.0313	0.0315	0.0314	0.0315	0.0316	0.0316	0.0316	0.0317	0.0317	0.0317
π	ECAL	0.0116	0.0126	0.0136	0.0138	0.0136	0.0136	0.0142	0.0144	0.0146	0.0151	0.0156
π	HCAL	0.0202	0.0226	0.0245	0.0267	0.0266	0.0268	0.0276	0.0280	0.0292	0.0298	0.0301

Table 7: Ratios of the energy deposited in sensitive layers to the incident energy for $\theta = 60°$ and no magnetic field.

Particle	Calorimeter	2 GeV	3 GeV	4 GeV	6 GeV	8 GeV	10 GeV	15 GeV	20 GeV	30 GeV	40 GeV	50 GeV
e^-	ECAL	0.0172	0.0173	0.0173	0.0174	0.0174	0.0174	0.0174	0.0174	0.0174	0.0174	0.0174
e^-	HCAL	0.0306	0.0308	0.0309	0.0310	0.0311	0.0312	0.0312	0.0312	0.0313	0.0313	0.0313
π	ECAL	0.0114	0.0127	0.0135	0.0138	0.0134	0.0135	0.0139	0.0143	0.0147	0.0150	0.0157
π	HCAL	0.0197	0.0223	0.0243	0.0265	0.0260	0.0265	0.0276	0.0282	0.0291	0.0295	0.0301

Table 8: Ratios of the energy deposited in sensitive layers to the incident energy for $\theta = 45°$ and no magnetic field.

Particle	Calorimeter	2 GeV	3 GeV	4 GeV	6 GeV	8 GeV	10 GeV
e^-	ECAL	0.0176	0.0177	0.0177	0.0177	0.0177	0.0177
π	ECAL	0.0115	0.0125	0.0131	0.0135	0.0134	0.0134
π	HCAL	0.0198	0.0227	0.0248	0.0265	0.0268	
Particle	Calorimeter	15 GeV	20 GeV	30 GeV	40 GeV	50 GeV	
e^-	ECAL	0.0177	0.0177	0.0178	0.0178	0.0178	
π	ECAL	0.0139	0.0141	0.0146	0.0149	0.0152	
π	HCAL	0.0278	0.0282	0.0289	0.0295	0.0299	

Table 9: Ratios of the energy deposited in sensitive layers to the incident energy for $\theta = 30°$ and no magnetic field.

5.2 Constant Magnetic Field

Figures 20 and 21 show the energy detected as a function of incident energy. As can be seen from comparing the plots of the ratio of energy deposited in the hadronic calorimeter to the incident energy with a magnetic field (Fig. 22 and 23) and without one (Fig. 18 and 19), the magnetic field does not affect the fraction of energy deposited in the endcaps ($\theta = 30°$ and $20°$). Particles that enter the hadronic calorimeter barrel ($\theta = 90°$, $60°$ and $45°$) deposit a larger fraction of their energy. The increase is approximately 7% for pions and 11% for electrons. The values of the ratios are shown in Tables 10-14.

Another interesting difference between the two types of simulations (with and without a magnetic field) is the dependence on the incident energy of the fraction of energy deposited by electrons in the hadronic calorimeter. When there is no magnetic field present, there seems to be no (or very little) dependence. However, when a magnetic field is present, the fraction of the energy deposited in the HCAL drops dramatically at lower energies (Fig. 23). The presence of the magnetic field does not significantly affect the energy deposition in the ECAL.

Particle	Calorimeter	2 GeV	3 GeV	4 GeV	6 GeV	8 GeV	10 GeV
e^-	ECAL	0.0164	0.0165	0.0166	0.0166	0.0167	0.0166
e^-	HCAL	0.0318	0.0337	0.0343	0.0347	0.0349	0.0350
π	ECAL	0.0109	0.0123	0.0130	0.0134	0.0130	0.0130
π	HCAL	0.0200	0.0235	0.0252	0.0276	0.0275	0.0281
Particle	Calorimeter	15 GeV	20 GeV	30 GeV	40 GeV	50 GeV	
e^-	ECAL	0.0167	0.0167	0.0167	0.0167	0.0167	
e^-	HCAL	0.0351	0.0352	0.0352	0.0353	0.0353	
π	ECAL	0.0135	0.0137	0.0141	0.0144	0.0150	
π	HCAL	0.0295	0.0296	0.0302	0.0314	0.0316	

Table 10: Ratios of the energy deposited in sensitive layers to the incident energy for $\theta = 90°$ and a 6 tesla magnetic field.

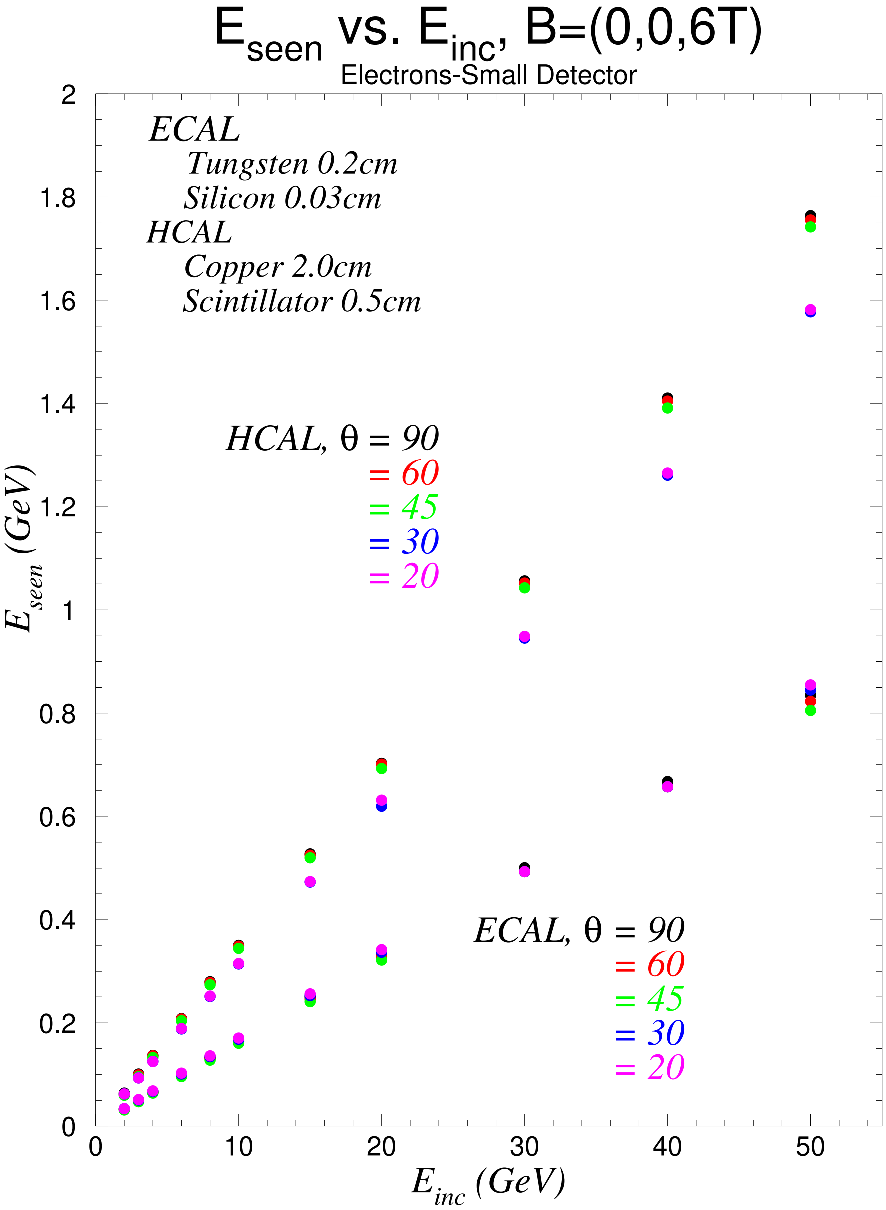

Figure 20: Energy detected by the sensitive layers in a 6 tesla magnetic field as a function of the incident energy of the electron.

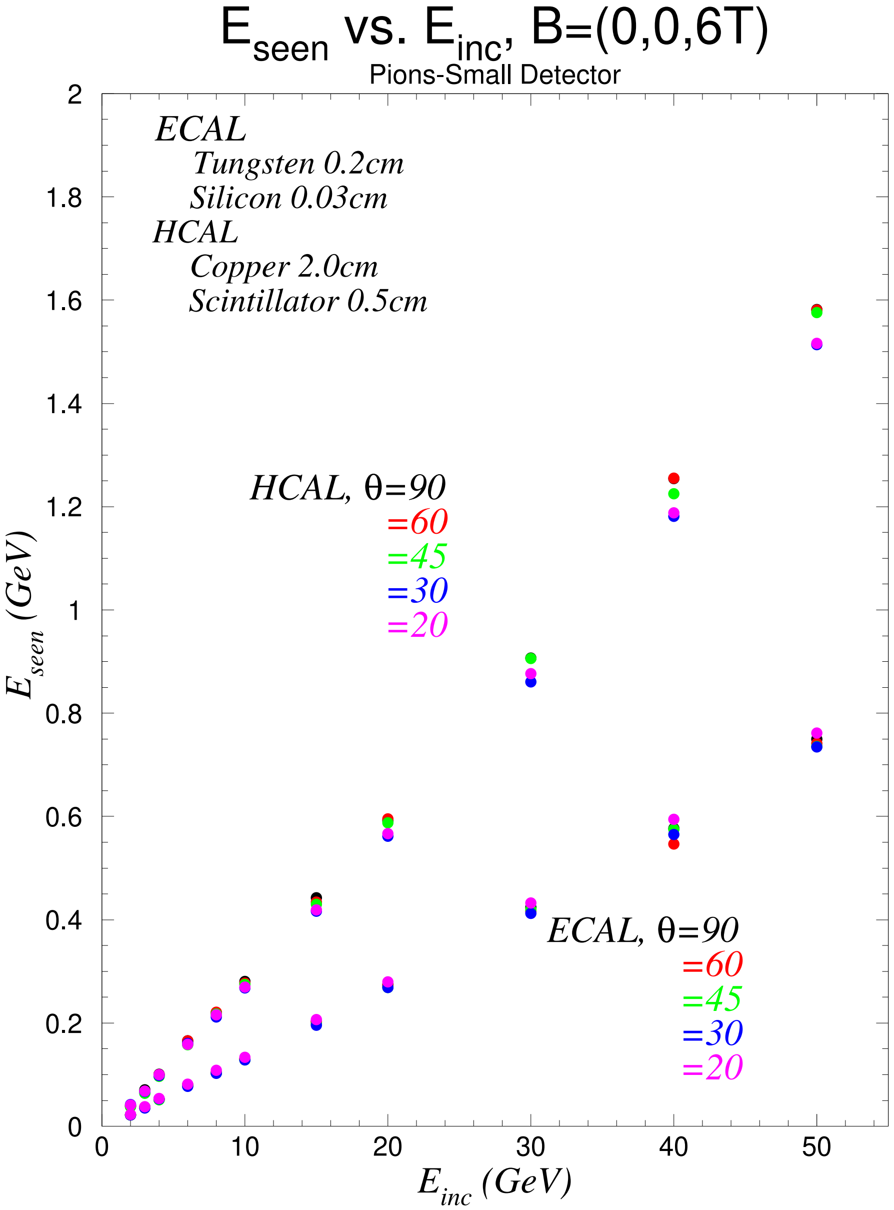

Figure 21: Energy detected by the sensitive layers in a 6 tesla magnetic field as a function of the incident energy of the pion.

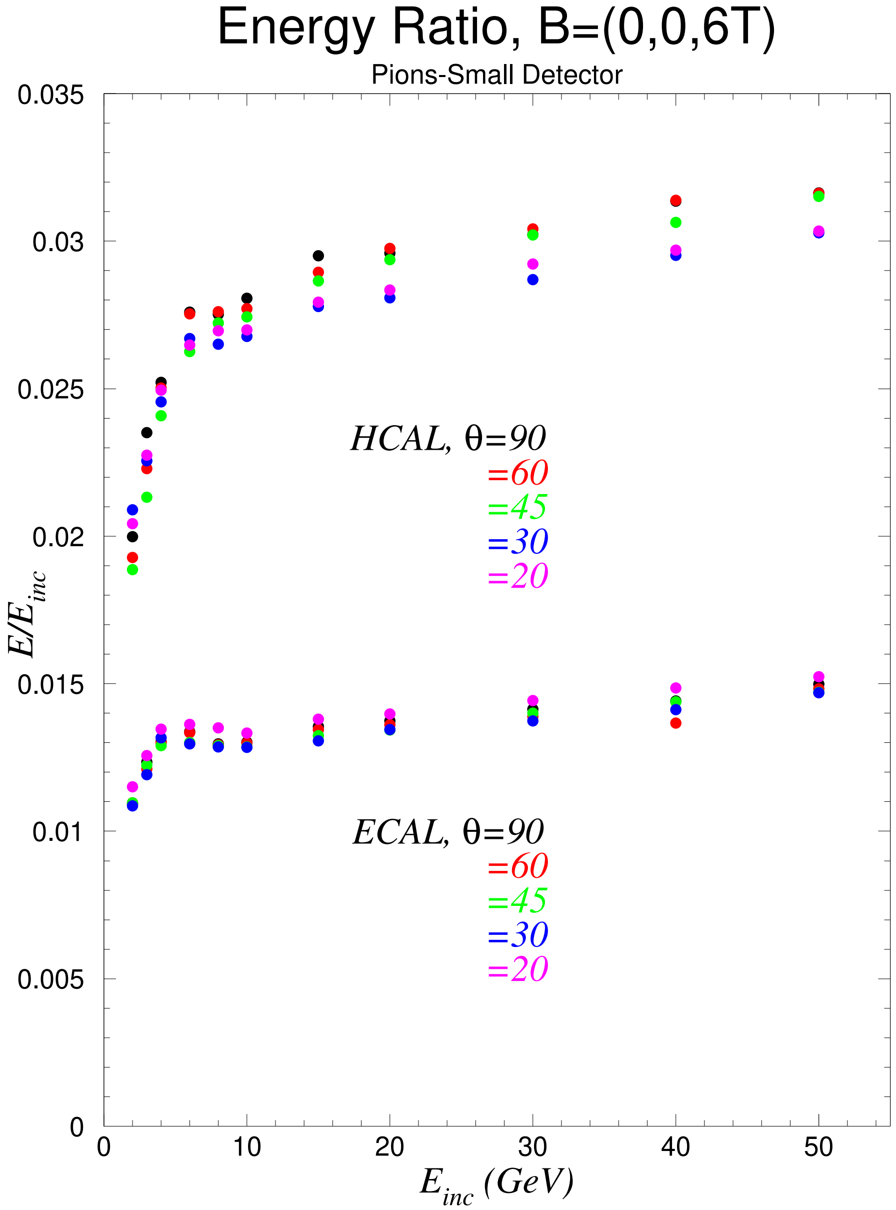

Figure 22: Ratio of the energy detected by the sensitive layers in a 6 tesla magnetic field to the incident energy of the pion.

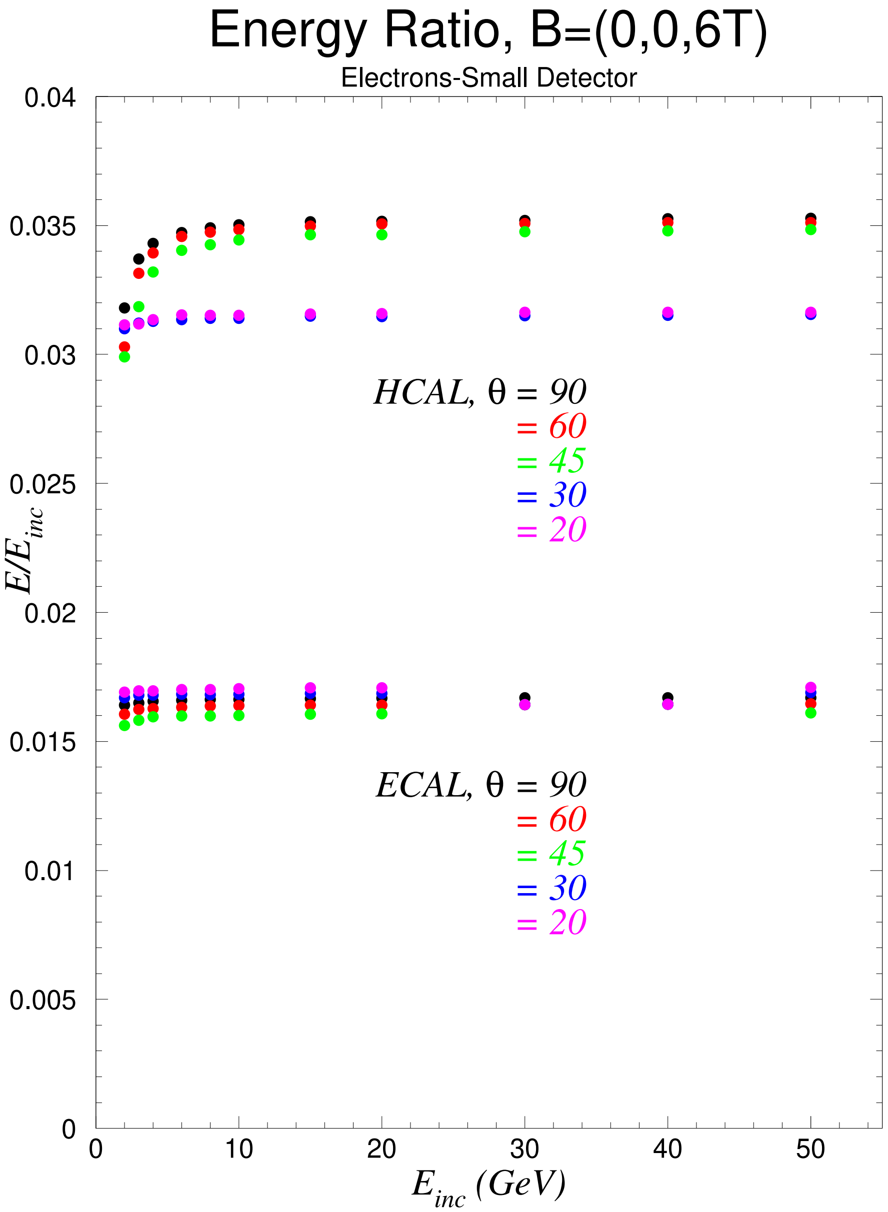

Figure 23: Ratio of the energy detected by the sensitive layers in a 6 tesla magnetic field to the incident energy of the electron.

Particle	Calorimeter	2 GeV	3 GeV	4 GeV	6 GeV	8 GeV	10 GeV	15 GeV	20 GeV	30 GeV	40 GeV	50 GeV
e^-	ECAL	0.0160	0.0162	0.0163	0.0163	0.0164	0.0164	0.0164	0.0164	0.0164	0.0164	0.0165
e^-	HCAL	0.0303	0.0331	0.0339	0.0346	0.0347	0.0348	0.0350	0.0351	0.0351	0.0351	0.0351
π	ECAL	0.0110	0.0121	0.0130	0.0133	0.0129	0.0130	0.0134	0.0136	0.0139	0.0137	0.0148
π	HCAL	0.0193	0.0223	0.0250	0.0275	0.0276	0.0277	0.0289	0.0298	0.0304	0.0314	0.0316

Table 11: Ratios of the energy deposited in sensitive layers to the incident energy for $\theta = 60°$ and a 6 tesla magnetic field.

Particle	Calorimeter	2 GeV	3 GeV	4 GeV	6 GeV	8 GeV	10 GeV	15 GeV	20 GeV	30 GeV	40 GeV	50 GeV
e^-	ECAL	0.0156	0.0158	0.0159	0.0160	0.0160	0.0160	0.0161	0.0161	0.0164	0.0164	0.0161
e^-	HCAL	0.0299	0.0318	0.0332	0.0340	0.0343	0.0344	0.0346	0.0346	0.0348	0.0348	0.0348
π	ECAL	0.0110	0.0122	0.0129	0.0130	0.0129	0.0129	0.0132	0.0134	0.0140	0.0144	0.0147
π	HCAL	0.0189	0.0213	0.0241	0.0263	0.0272	0.0274	0.0286	0.0294	0.0302	0.0306	0.0315

Table 12: Ratios of the energy deposited in sensitive layers to the incident energy for $\theta = 45°$ and a 6 tesla magnetic field.

Particle	Calorimeter	2 GeV	3 GeV	4 GeV	6 GeV	8 GeV	10 GeV	15 GeV	20 GeV	30 GeV	40 GeV	50 GeV
e^-	ECAL	0.0167	0.0168	0.0168	0.0168	0.0168	0.0168	0.0169	0.0169	0.0164	0.0164	0.0169
e^-	HCAL	0.0310	0.0312	0.0313	0.0314	0.0314	0.0314	0.0315	0.0315	0.0315	0.0315	0.0315
π	ECAL	0.0209	0.0226	0.0245	0.0267	0.0265	0.0268	0.0278	0.0281	0.0287	0.0295	0.0303
π	HCAL	0.0109	0.0119	0.0132	0.0130	0.0129	0.0128	0.0131	0.0134	0.0137	0.0141	0.0147

Table 13: Ratios of the energy deposited in sensitive layers to the incident energy for $\theta = 30°$ and a 6 tesla magnetic field.

Particle	Calorimeter	2 GeV	3 GeV	4 GeV	6 GeV	8 GeV	10 GeV	15 GeV	20 GeV	30 GeV	40 GeV	50 GeV
e^-	ECAL	0.0169	0.0170	0.0170	0.0170	0.0170	0.0170	0.0170	0.0170	0.0164	0.0164	0.0171
e^-	HCAL	0.0312	0.0312	0.0313	0.0315	0.0315	0.0315	0.0316	0.0316	0.0316	0.0316	0.0316
π	ECAL	0.0115	0.0126	0.0135	0.0135	0.0135	0.0133	0.0138	0.0140	0.0144	0.0149	0.0152
π	HCAL	0.0204	0.0227	0.0249	0.0265	0.0270	0.0270	0.0279	0.0283	0.0292	0.0297	0.0303

Table 14: Ratios of the energy deposited in sensitive layers to the incident energy for $\theta = 20°$ and a 6 tesla magnetic field.

6 Conclusion

I used a computer simulation package called GEANT to produce realistic results of electrons and pions interacting with the Small detector geometry. Working on the computer simulation allowed me to produce important results in the research and development of the next international linear collider detector. My resolution results are compared with those of an independent, yet very similar study being done at the Stanford Linear Accelerator Center. These studies are providing information as well as revealing problems that must be dealt with.

The addition of a magnetic field does not have a great adverse effect on the resolution and energy deposition (and thus calibration). By comparing my results with those of another group member, Aaron Preston, who is simulating a detector with lead instead of copper, we conclude that using thick layers of copper is a poor choice. Copper causes the drop in the fraction of energy deposited for pion energies $\lesssim$ 6 GeV. Also, the copper causes the resolution to be nonlinear in $1/\sqrt{E}$ at low energies ($\lesssim$ 2 GeV).

I measured values of the resolution in the expected range with reasonable errors. Section 4 gives a summary of resolution slopes and intercepts for the Small detector and the calibration is discussed in Section 5.

Future work will include resolution and calibration studies with a more realistic magnetic field and simulating the calorimeters together using the proper number of layers. In the more distant future, the same questions studied here must be asked for other possible detector geometries and materials.

A Resolution of a Sampling Calorimeter

A sampling calorimeter is one that is made of alternating sensitive and non-sensitive layers and thus *samples* the particles energy. Finding the energy dependence of the resolution (σ/μ) may be done with an example.

First I must briefly discuss critical energies and radiation lengths. Electrons may loose energy by ionization and bremsstrahlung. As incident energy increases, energy loss by ionization drops off and energy loss by bremsstrahlung increases [3]. The energy at which these two losses are equal is called the critical energy, E_c.

For high energy electrons and photons ($E \gg 10$ MeV), the change in energy, dE, in a length of material, dx, is proportional to the energy of the particle, E.

$$\begin{aligned} \frac{dE}{dx} &= E/X_0 & \text{(A.1)} \\ E(x) &= E_0 e^{-x/X_0} & \text{(A.2)} \end{aligned}$$

This defines the radiation length, X_0. It is the length in which the energy of a beam of particles drops to $\frac{1}{e} \approx 37\%$ of its original value.

Imagine that a photon or an electron enters a material and after each radiation length, two particles are created. This means that each photon will pair produce and each electron (or positron) will bremsstrahlung as described in Section 2.2. Assume further that each child particle splits the energy of the parent particle evenly. If this is so, the number of particles at depth x (measured in radiation lengths) is

$$N(x) = 2^x$$

and the energy of each particle at that depth is,

$$E(x) = E_0 \cdot 2^{-x}.$$

This EM shower continues until the energy of each of the particles is less than the critical energy, E_c. At that point, the shower attenuation is quite large. The depth at which this happens is called the shower maximum, x_{max} and is

$$x_{\text{max}} = \frac{\ln(E_0/E_c)}{\ln 2} \tag{A.3}$$

The total number of particles in the shower is

$$\begin{aligned}
N_{\text{tot}} &= \sum_{x=0}^{x_{\max}} 2^x \\
2N_{\text{tot}} &= \sum_{x=0}^{x_{\max}} 2^{x+1} \\
N_{\text{tot}} - 2N_{\text{tot}} &= \sum_{x=0}^{x_{\max}} 2^x - \sum_{x=0}^{x_{\max}} 2^{x+1} = 1 - 2^{x_{\max}+1} \\
N_{\text{tot}} &= \frac{1 - 2^{x_{\max}+1}}{1-2} = 2 \cdot 2^{x_{\max}} - 1 \\
N_{\text{tot}} &= 2 \cdot \frac{E_0}{E_c} - 1 \approx 2\frac{E_0}{E_c} \\
N_{\text{tot}} &\propto E_0 \qquad \text{(A.4)}
\end{aligned}$$

The total track length (the sum of the distances traveled by *all* particles), x_{tot}, is

$$x_{\text{tot}} = X_0 N_{\text{tot}} \qquad \text{(A.5)}$$

Because a sampling calorimeter only records energy deposition where there are sensitive materials, the total number of samplings, is

$$N_{\text{samp}} = \frac{x_{\text{tot}}}{x_{\text{samp}}} = \frac{X_0 N_{\text{tot}}}{x_{\text{samp}}} \qquad \text{(A.6)}$$

where x_{samp} is the distance between sensitive layers.

The total amount of energy deposited, E_{dep}, is the sum of the energy deposited at each sampling, ϵ_i.

$$E_{\text{dep}} = \sum_{i=1}^{N_{\text{samp}}} \epsilon_i \qquad \text{(A.7)}$$

According to the Central Limit Theorem, the standard deviation, σ, of a sum (and thus the distribution of deposited energies, E_{dep}), goes as the square root of the number of data points, $\sqrt{N_{\text{samp}}}$ [5].

$$\sigma_{E_{\text{dep}}} \propto \sqrt{N_{\text{samp}}} \qquad \text{(A.8)}$$

For a sampling calorimeter, we may then expect that

$$\frac{\delta E_{\mathrm{dep}}}{E_{\mathrm{dep}}} \equiv \frac{\sigma_{E_{\mathrm{dep}}}}{E_{\mathrm{dep}}} \propto \frac{\sqrt{N_{\mathrm{samp}}}}{N_{\mathrm{samp}}} = \frac{1}{\sqrt{N_{\mathrm{samp}}}} \tag{A.9}$$

Therefore, using equations A.4 and A.6 we obtain the desired result.

$$\frac{\delta E_{\mathrm{dep}}}{E_{\mathrm{dep}}} \propto \frac{1}{\sqrt{E_0}} \tag{A.10}$$

B Resolution Error Analysis

Resolution errors propagate from the measurement of the mean and standard deviation of the energy distributions. Propagation of errors allows us to find the errors of the intercept, a, and the slope, b, from equation 4.1. Equation B.1 shows the propagation of errors for an arbitrary function, $q(x_1, x_2, \ldots, x_n)$.

$$\delta q(x_1, x_2, \ldots, x_n) = \sqrt{\left(\frac{\partial q}{\partial x_1}\delta x_1\right)^2 + \left(\frac{\partial q}{\partial x_2}\delta x_2\right)^2 + \cdots + \left(\frac{\partial q}{\partial x_n}\delta x_n\right)^2} \tag{B.1}$$

The independent variable for the linear fit we are interested in is $x = 1/\sqrt{E}$ and the dependent variable is $y = \sigma/\mu$ (see Sec. 4). It can be shown that the intercept and slope of the least squares line of best fit to N data points is given by equations B.2 and B.3, respectively [5].

$$a = \frac{(\Sigma x^2)(\Sigma y) - (\Sigma x)(\Sigma xy)}{\Delta} \tag{B.2}$$

$$b = \frac{N(\Sigma xy) - (\Sigma x)(\Sigma y)}{\Delta} \tag{B.3}$$

$$\Delta \equiv N\left(\Sigma x^2\right) - (\Sigma x)^2$$

Equation B.1 is applied because we are interested in finding the error in the slope and intercept of the line of best fit in terms of the (known) errors in the measured mean, μ, and standard deviation, σ. Because a and b are functions of the dependent variable, σ/μ, it follows that the errors in the slope and intercept are:

$$\delta a = \sqrt{\sum_k \left(\frac{\partial a}{\partial y_k}\delta y_k\right)^2} \tag{B.4}$$

$$\delta b = \sqrt{\sum_k \left(\frac{\partial b}{\partial y_k}\delta y_k\right)^2} \tag{B.5}$$

By differentiating equations B.3 and B.2 with respect to an arbitrary dependent variable, y_k, we find,

$$\begin{aligned}\frac{\partial a}{\partial y_k} &= \frac{\Sigma x^2}{\Delta}\left(\frac{\partial}{\partial y_k}\sum_i y_i\right) - \frac{\Sigma x}{\Delta}\left(\frac{\partial}{\partial y_k}\sum_i x_i y_i\right)\\ \frac{\partial b}{\partial y_k} &= \frac{N}{\Delta}\left(\frac{\partial}{\partial y_k}\sum_i x_i y_i\right) - \frac{\Sigma x}{\Delta}\left(\frac{\partial}{\partial y_k}\sum_i y_i\right)\end{aligned}$$

Because each of the y_k's are independent measurements, $\frac{\partial y_i}{\partial y_j} = \delta_{ij}$. Therefore,

$$\begin{aligned}\frac{\partial}{\partial y_k}\sum_i x_i y_i &= x_k\\ \frac{\partial}{\partial y_k}\sum_i y_i &= 1\end{aligned}$$

Using the derivatives just found in equations B.4 and B.5 we obtain the final result. Equations B.6 and B.7 are used to calculate the error in the resolution fits. The summations are easily handled from a programming standpoint.

$$\delta a = \sqrt{\sum_k \left[\left(\frac{\sum_i x_i^2}{\Delta} - \frac{x_k \sum_i x_i}{\Delta}\right)(\delta y_k)\right]^2} \tag{B.6}$$

$$\delta b = \sqrt{\sum_k \left[\left(\frac{N x_k}{\Delta} - \frac{\sum_i x_i}{\Delta}\right)(\delta y_k)\right]^2} \tag{B.7}$$

Because $y = \sigma/\mu$,

$$\delta y_k = \sqrt{\left(\frac{\partial y}{\partial \sigma}\delta\sigma_k\right)^2 + \left(\frac{\partial y}{\partial \mu}\delta\mu_k\right)^2}$$

References

[1] Howard E. Haber and G.L. Kane. The search for supersymmetry: Probing physics beyond the standard model. 1984. Physics Reports 110.

[2] *Physics and Technology of the Next Linear Collider: A Report Submitted to Snowmass '96*, June 1996. hep-ex/9605011.

[3] Claus Grupen. *Particle Detectors.* Number 0-521-55216-8. Cambridge University Press, Cambridge, England, 1996.

[4] Thomas Ferbel. *Experimental Techniques in High Energy Physics.* Number 0-201-11487-9. Addison-Wesley Publishing Company, Inc., Menlo Park, California, 1987.

[5] Jay L. Devore. *Probability and Statistics for Engineering and the Sciences.* Number 0-534-24264-2. Wadsworth Publishing Company, Belmont, CA, 1995.